Damage Prediction in Fiber Reinforced Composites

Jabir Ubaid P

A Dissertation Submitted to
Indian Institute of Technology Hyderabad
In Partial Fulfillment of the Requirements for
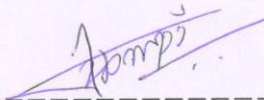The Degree of Master of Technology

भारतीय प्रौद्योगिकी संस्थान हैदराबाद
Indian Institute of Technology Hyderabad

Department of Mechanical Engineering

June, 2013

Declaration

I declare that this written submission represents my ideas in my own words, and where others' ideas or words have been included, I have adequately cited and referenced the original sources. I also declare that I have adhered to all principles of academic honesty and integrity and have not misrepresented or fabricated or falsified any idea/data/fact/source in my submission. I understand that any violation of the above will be a cause for disciplinary action by the Institute and can also evoke penal action from the sources that have thus not been properly cited, or from whom proper permission has not been taken when needed.
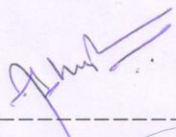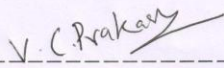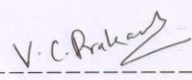
_____

Jabir Ubaid

ME11M06

Approval Sheet

This thesis entitled Damage prediction in fiber reinforced composites by Jabir Ubaid P is approved for the degree of Master of Technology from IIT Hyderabad.
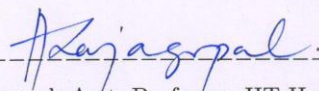
_____

Dr. Abhay Sharma, Asst. Professor, IIT Hyderabad

Examiner

_____

Dr. Chandrika Prakash Vyasarayani, Asst. Professor, IIT Hyderabad

Examiner

_____ (on behalf of Dr Ramji)

Dr. M. Ramji, Asst. Professor, IIT Hyderabad

Adviser

_____

Dr. Amirtham Rajagopal, Asst. Professor, IIT Hyderabad

Chairman

iii

Acknowledgements

Dedicated to

My parents and siblings

Abstract

Various failure modes can occur in a composite laminate subjected to external load. With the increasing external load, the failure evolves in composite laminate and evolution behavior depends on the failure modes. Thus, the knowledge of the damage mechanisms in composite laminate plays an important role in the practical design of composite structures. The stiffness degradation phenomenon of fiber reinforced composite laminates under external loads is an important response to the damage and failure evolution of composite laminates. The analysis of stiffness degradation of composite laminates under external load is called as the progressive failure analysis. In this work, a 3D finite element based progressive damage model is developed for fiber reinforced composite laminates and it is applied to CFRP laminates having multiple holes and also to multi-pin joints in CFRP laminates. The developed model is suitable for predicting failure and post failure behavior of the laminates. The PDM involves stress analysis, failure analysis and damage propagation. Digital image correlation experiment is carried out to perform whole field surface strain analysis of the composite laminates. Finite element model is validated by comparison of whole field surface strain and displacement from finite element prediction with digital image correlation results. The failure modes predicted by PDM is found to be in good agreement with experimental observation. Also load-deflection behavior predicted by both PDM simulation and experiment are found to be in good agreement thereby confirming the accuracy of PDM implementation. Effect of spacing between the holes on the maximum stress value in the panels is also further investigated.

Nomenclature

CFRP	Carbon fiber reinforced polymer
PDM	Progressive damage modeling
PFA	Progressive failure anlaysis
DIC	Digital image correlation
FEA	Finite element analysis
MPDM	Material property degradation method
gsm	Grams/square meter
SCF	Stress concentration factor
u	Component of displacement in x direction
ε_{ij}	Component of strain in the respective directions
σ_{ij}	Component of stress in the respective directions

Contents

List of Figures

1

2

List of Tables

Chapter 1
Introduction and Literature Review

1.1   Introduction

In the competitive environment of aircraft industries it becomes absolutely necessary to improve the efficiency, performance of the aircrafts to reduce the development and operating costs considerably, in order to capitalize the market. An important contribution to improve the efficiency and performance can be achieved by decreasing the aircraft weight through considerable usage of composite materials in primary aircraft structures. Advanced fiber reinforced composite materials were originally developed for aerospace industry to use as primary structural materials. All the major aircraft manufacturers have been trying to develop the next generation of airliners using more amounts of composite materials. This trend is expected to continue well into the future with significant improvement in fuel economy among other benefits. New generation of aircrafts tend to use thicker laminates carrying more loads. Commercial aircrafts such as the Boeing 757, 767 and 777 rely on composites in their control surfaces, ailerons, flaps, elevators, and rudders, and in their wing/body fairings and engine nacelles. In the Airbus family, and the Boeing 777, the vertical and horizontal stabilizers are also of carbon fiber construction. Figure 1.1 shows the trend of increasing use of composites and decreasing use of aluminum alloys in Boeing aircrafts. The Boeing 787 Dreamliner makes greater use of composite materials than any previous commercial airliner. Up to 50% of the Boeing 787 Dreamliner aircraft is built using carbon fiber reinforced plastic and other composites including the fuselage and wings. A350 XWB has roughly 53 % of composites utilized in the fuselage and wing. The use of composite materials in Boeing 787 Dreamliner aircraft is illustrated Figure 1.2. Fiber reinforced plastics continue to replace traditional metallic materials in structural components not only in aerospace industry but also in various other industries that demand a high level of mechanical performance like sports, rapid transit railway, marine, automotive, biomedical etc..
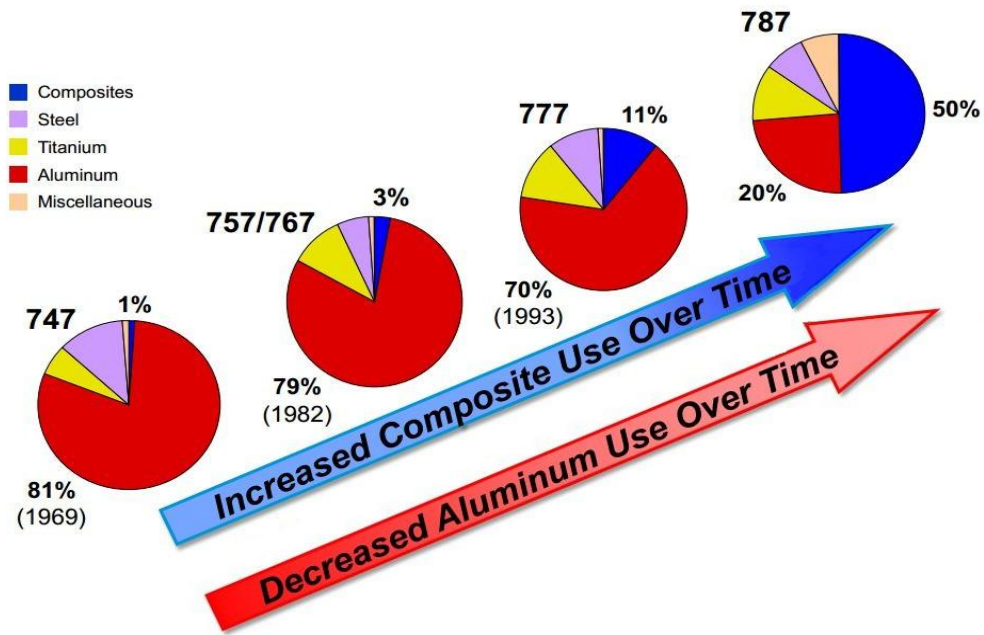
Figure 1.1: Trend of material usage in Boeing aircrafts [1]
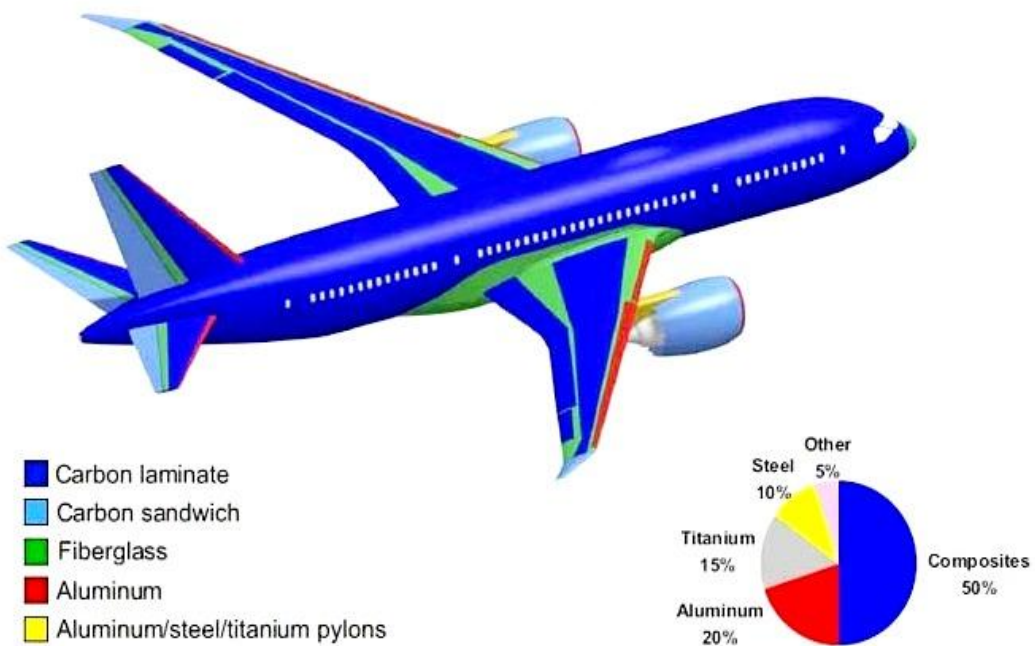
Figure 1.2: Breakdown of materials used in Boeing 787 Dreamliner [1]

Fiber reinforced composite materials are distinguished by their extremely high strength and modulus besides various other benefits such as low density, corrosion resistance, high fatigue life etc. Despite their excellent physical properties, CFRP is fragile and susceptible to damage because of its inherent brittle nature. When subjected to high service loads, environmental attack or a combination of any or all of the above, CFRP laminates develop a complicated failure mechanism. Increased use of CFRP in structural parts with high mechanical property needs better understanding about the mechanical behavior of CFRP structures.

Figure 1.3: Wing covers of Airbus A350 XWB made of CFRP [2]

1.1.1 Multiple holes in composite structures

Most of the structures need the presence of multiple holes and cut-outs in them mainly for joining of different structural parts, damage inspection and for installation of electrical and hydraulic piping system etc. [3, 4]. Such holes are source of stress raisers due to geometrical discontinuity and act as site of damage initiation. Stresses around the hole are three dimensional by nature due to the presence of interlaminar stresses at free edges. The presence of multiple interacting holes makes the problem still more complex. The failure mechanism and strength prediction of such structures is of great interest mainly because of practical applications. Figure 1.3 shows the wing covers of Airbus A350 XWB made from CFRP with multiple cut-outs.

1.1.2 Mechanically fastened joints in composite structures

Due to strength and safety requirements, the applications of composites require joining composites either to composites or to metals. Even though, there are disadvantages such as weight addition and stress concentration due to geometric discontinuity, mechanical fasteners are widely used in the aerospace industry. Figure 1.4 shows mechanically fastened joint in composite fuselage part of Boeing 787. Mechanically fastened joints (such as pinned joints) are unavoidable in complex structures because mechanically fastened joints can be easily disassembled without damage, do not need surface preparation for joining and are easy to inspect. The basic method of mechanical joining is done by drilling holes in the two materials to be joined (such as two composite laminates) and then placing a mechanical fastener through the holes and fixing the fastener in place. The types of fasteners usually dictate the fixing method. Bolts are fixed with nuts, screws are fixed through the interaction of the threads and the materials to be bonded, rivets are fixed by heading the rivet itself, and pins are fixed by simple interference with the holes. Because these methods do not rely upon the nature of the surfaces of the materials being joined, little or no surface preparation is required. The only dependence on the materials is the strength of the materials at the joint location. For e.g., if the materials are week in compression, the compressive force excreted by bolts and nuts could lead the materials to deform. Also, if the materials are not strong in shear, screws may not hold.

Joint efficiency has been a major concern in using laminated composite materials. Relative inefficiency and low joint strength have limited widespread application of composites. Durable and strong composite joint is an urgent need for the primary structural members made of composite laminates. Because of the anisotropic and heterogeneous nature, the joint

behavior in composites is more difficult to analyze than the case with isotropic materials. As efficiency of the structure increases because of better design of joints, the operational load continues to grow and the load carried by each fastener increases accordingly. This increases probability of failure. Therefore, the assessment of the stresses around the fasteners holes becomes critical for damage-tolerant design. Because of the presence of unknown contact stresses and contact region between the fastener and the laminate, the analysis of a pin-loaded hole becomes considerably more complex than that of a traction-free hole [5]. Improper design of the joints may lead to structural problems or conservative design leading indirectly to overweight structures and high life-cycle cost of the aircraft. The accurate prediction of the stress distribution along the hole edge is essential for reliable strength evaluation and failure prediction. The knowledge of the failure strength would help in selecting the appropriate joint size in a given application. Progressive damage analysis is important in order to understand the failure process and to calculate the maximum load capacity of a joint under an overload situation.
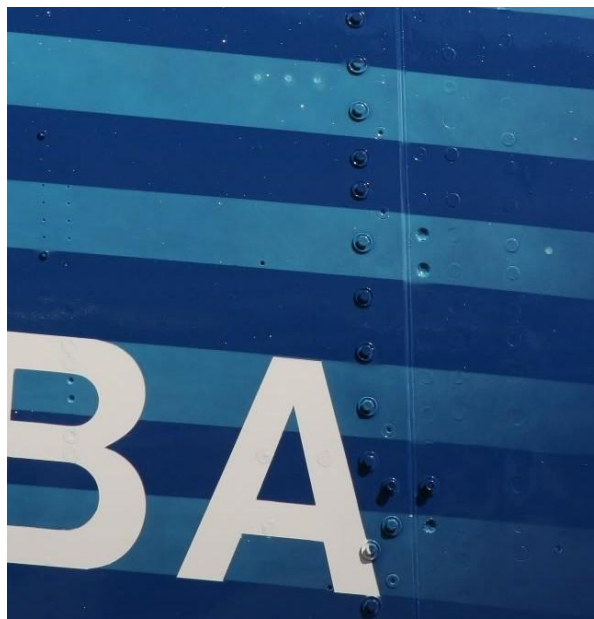
Figure 1.4: Mechanically fastened joint in Boeing 787 fuselage [6].

1.1.3   Progressive failure analysis of composite laminates

The failure mechanism in composite structures is very complicated compared to traditional metallic materials. Unlike conventional metallic materials, composite structures fail under different localized failure modes such as matrix cracking, matrix shear failure, fiber breakage, fiber kinking and delamination which are shown in Figure 1.5. Figure 1.6 shows the SEM micrographs of the fracture surface of fiber reinforced plastics failed under

9

different failure modes. These failure modes result in a loss in strength and stiffness of composite materials, and sometimes may lead to catastrophic disasters. The different failure modes together with inhomogeneity and anisotropic nature of composites make prediction of strength and failure mechanism of them very challenging. Accurate determination of failure modes and the failure progression will be useful for the betterment of design of composite structures and for defining fail safe criteria. Since sufficient tests on composite materials to predict strength and failure mechanism are time consuming and very expensive to perform, predictive tools based on computational methods such as finite element method (FEM) are getting wide acceptance. The stiffness degradation phenomenon of fiber reinforced composite laminates under continuous load is an important response to the damage initiation and evolution of composite laminates and the corresponding analysis is termed as the progressive failure analysis [7].
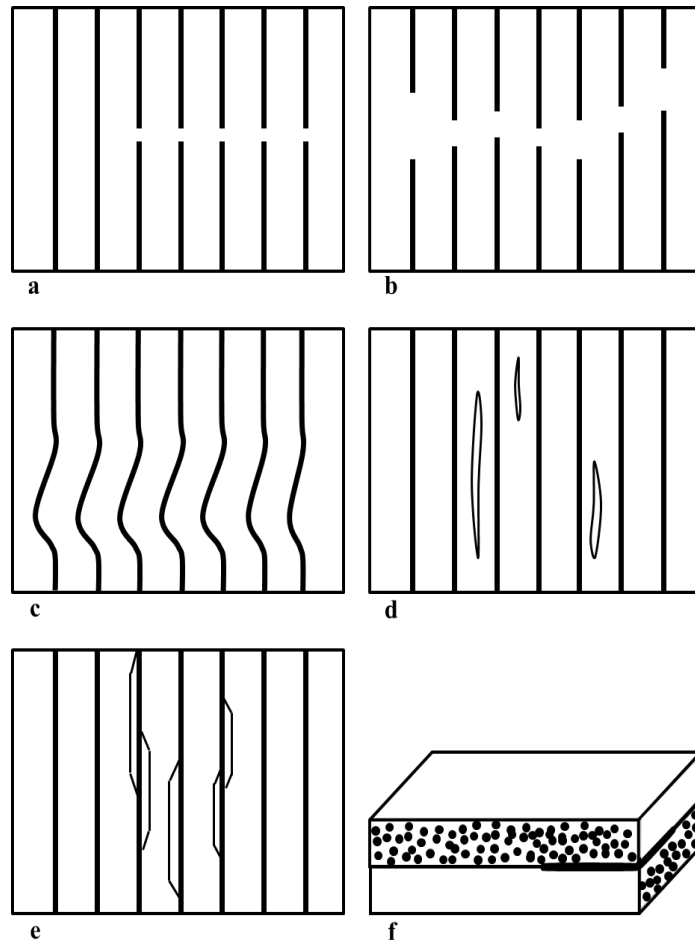
Figure 1.5: Schematic representation of failure modes is fiber reinforced composites (a) Fiber failure (b) Fiber pull out (c) Fiber kinking (d) Matrix cracking (e) Fiber matrix de-bonding (f) Delamination

10

In this study, a generic 3D linear finite element based progressive damage model for CFRP unidirectional laminate is developed and applied for a CFRP panel having multiple holes and also for multi-pin joints in CFRP panels being subjected to tensile load. The model is capable of predicting the onset of damage, damage progression and the post failure response. Whole field surface strain as well as displacement distribution is obtained from digital image correlation (DIC) experiments and they are compared with the finite element model prediction to validate the PDM. Load-displacement behavior is captured from the experiment and is compared with those predicted by PDM. Experimentally, damage mechanism is looked at and compared with the PDM prediction.
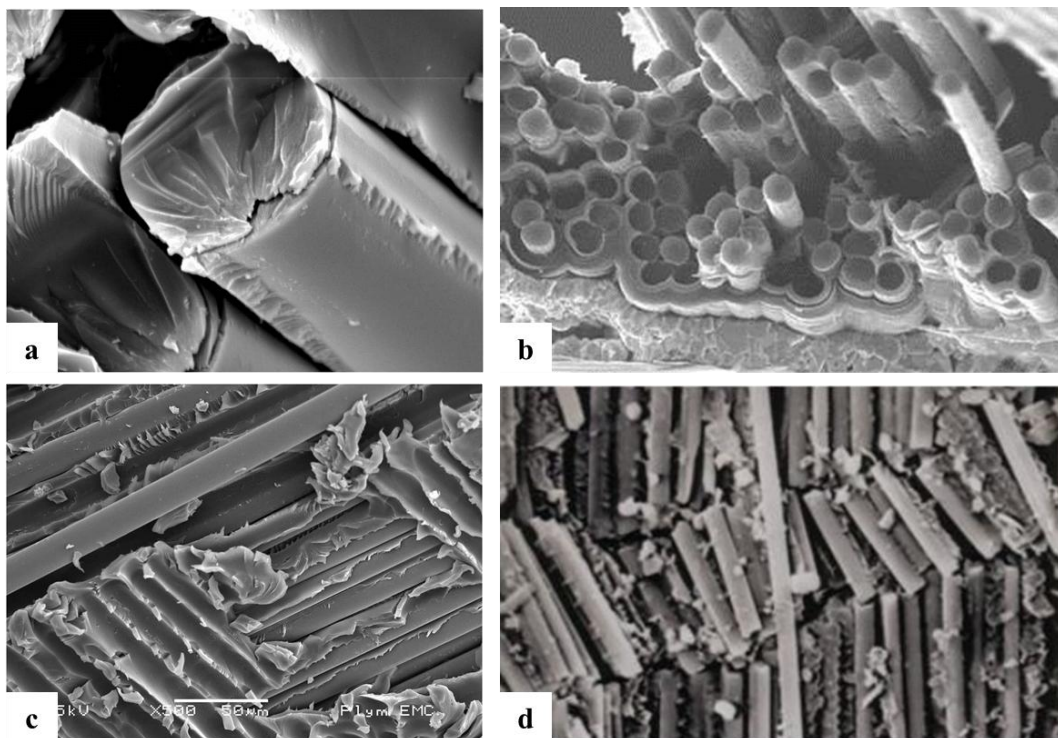
Figure 1.6: SEM micrographs of fracture surface of fiber reinforced plastics failed under different failure modes (a) Fiber failure (b) Fiber pull out (c) De-bonding between fiber and matrix (d) Micro buckling of fiber [8]

1.1.4   Failure criteria for composite materials

In order to use fibrous composite materials effectively as structural elements, designers need to predict the conditions under which the composite materials will fail. Also, failure prediction is an integral part of any progressive damage model. For this purpose, numerous failure theories for fibrous composites have been proposed. Most of these theories are developed by extending the well-established failure theories for isotropic materials to account for the anisotropy in stiffness and strength of the composites. These criteria can be

11

classified in a number of ways, including whether they are based on strength or fracture mechanics theories, whether they predict failure in a general sense or are specific to a particular failure mode, and whether they focus on in-plane or inter-laminar failure [9].

In situ strengths are used in a number of failure criteria, though the method for determining these values varies between papers. In situ strengths are used as it has been found experimentally that a ply embedded within a multi-directional laminate has increased transverse tensile and shear strengths as compared to the same ply in a completely unidirectional laminate [10]. This is due to the beneficial effect of the neighboring plies on damage within an embedded ply, and means that values taken from standardized experimental characterization coupons, which all use unidirectional coupons, can underestimate actual ply strengths. Orifice et al. [9] have published a detailed study on failure criteria that have been specifically developed for fiber reinforced composites.

Several researchers have proposed failure criteria in which the separate failure modes are not considered, and failure of the entire ply is predicted [11, 12]. This group includes criteria from papers in which the difference between fiber and matrix failure is either unclear or not specified such as Tsai and Wu criterion [9], in which all the strength data is used to create a failure surface, usually in stress space. Ply failure criteria are more suited and almost always applied in situations where delamination can be ignored. It is interesting to note that interactive criteria such as Tsai–Wu are often criticized due to their lack of phenomenological basis and origins in theories originally proposed for metals [9]. However, interactive criteria have demonstrated accuracy comparable with leading theories in which the failure modes are considered, and continue to be commonly applied in industry and widely available in FE codes [13].

Below is a brief description about various failure criteria that can be used for predicting different modes of failure in fiber reinforced composites.

1.1.4.1 Fiber failure

Fiber failure in tension usually occurs due to the accumulation of individual fiber failures within plies in the composite laminates. This becomes critical when there are not enough intact fibers remaining to carry the required loads. Most of the studies carried out to analyse fiber failure in tension include using maximum strength or maximum strain criterion. It involves checking maximum stress or strain values against simple material limit values taken from experimental results. Exceptions to this include Hashin [14] who uses a quadratic interaction criterion involving in-plane shear, Chang and Chang [15] who apply

the Hashin quadratic interaction criterion but incorporate nonlinear shear behavior, and Puck and Schürmann [16] used a maximum strain criterion with a stress magnification factor applied to transverse normal stress.

Micro buckling and the formation of kink bands are the main reasons for fiber failure in compression, and though there is still debate over whether these phenomena are separate failure modes, micro buckling is a more global failure mode whilst kinking seems to be initiated by local microstructural defects and is the most common failure feature observed after testing [9]. Many researchers have applied the maximum stress or maximum strain criteria using limit values from experimental characterization to find out fiber failure in compression, though a number of approaches have been developed for incorporating the effects of micro buckling and kinking [10, 15-16]. Few researchers have developed failure criteria for fiber failure in which the different tension and compression properties of the ply are not specified, combined within the one criterion, or not considered [17].

1.1.4.2 Matrix failure

Matrix failure in laminated composites is a complex phenomenon. Matrix cracks initiate typically at defects or fiber– matrix interfaces, accumulate throughout the laminate, and coalesce leading to failure across a critical fracture plane [9]. Numerous researchers have developed approaches for predicting the initiation and evolution of matrix cracks, using different approaches.

All the criteria developed for matrix failure in tension assume a critical fracture plane in the transverse tension direction, and generally involve an interaction between the tensile normal and in-plane shear stresses. Apart from the maximum stress and maximum strain criteria, the simplest proposal is the quadratic interaction criterion of Hashin [14], and further developments include nonlinear shear terms, in situ transverse tensile and shear strengths, incorporating crack density, the use of through-thickness shear and strength terms (in the 23 direction), and the inclusion of fracture mechanics terms from a consideration of a cracked ply [18]. An exception to this is the criterion of Cuntze and Freund [11], which is only based on the transverse tensile stress and strength and through-thickness shear stress   .

The criteria for matrix failure in compression are similar to those for tension failure, except that the critical fracture plane is not assumed by all authors. Hashin and Rotem [19] assumed the fracture plane is in the transverse direction and proposed a simple quadratic interaction criterion using the transverse normal and in-plane shear components. This is then modified by Hashin [14] to include the through-thickness strength. In contrast, the criterion

of Cuntze and Freund [11] uses only the transverse normal strength, with a combination of several stress invariants. There are some criteria for matrix failure in which the different tension and compression properties of the ply are not specified, combined within the one criterion, or not considered [17].

1.1.4.3 Shear failure

There are number of criteria that can be applied in analyzing in-plane shear failure. Maximum strength or maximum strain criterion is widely used. It involves checking maximum stress or strain values against simple material limit values taken from experimental results. Hashin [14] can be used to analyse fiber–matrix shear failure. Several modifications such as incorporating nonlinear shear or matrix crack density is made by various researchers. It is interesting to note that the choice of tension or compression strength is not consistent between papers. Also, a criterion is developed by Cuntze and Freund [11], in which the in-plane shear strength is used with a number of stress invariants.

1.1.4.4 Delamination

A number of criteria have been proposed to predict the initiation and evolution of delamination using the stress values of an individual ply or interface element (meshed between plies) [14, 20]. These criteria all use combinations of the through-thickness tensile and shear parameters, in linear, quadratic or curve-fit relationships, with a small number also considering the stress in the fiber direction [21]. An exception to this is the approach of Wisnom et al. [22], which is based on using principal stresses.

1.1.5   Experimental techniques for strain measurement in composite laminates

There are many experimental techniques which have evolved over years to address the issue of accurate measurement of surface strain and damage detection in the composite panel. Aside from the widely used point wise strain gauge technique which is a highly localized strain measurement technique, various full-field non-contact optical methods, including both interferometric techniques and non-interferometric techniques have been developed and applied for this purpose. The improvement in image processing with microcomputers has caused non-contact measurement techniques to become more and more popular in the experimental mechanics community [23]. In the recent past, thanks to the dramatic advances in microcomputer and camera technology, many research groups devoted to optics, experimental mechanics or data processing have been developing suitable techniques based on the use of optical devices, digital cameras, algorithms and software which automatically process images. These techniques directly provide displacement or strain contours onto

specimens under testing. In case of interferometry techniques, electronic speckle pattern interferometry (ESPI), moiré interferometry and reflection photoelasticity are commonly employed [24, 25-26]. Reflection photoelasticity involves bonding of a reflective coating layer on the specimen. It is not a straight forward process and it needs expertise to bond the coating layer on the specimen. All these interferometric methods require a coherent light source, and the measurements are normally conducted in a vibration-isolated optical platform in the laboratory. Interferometric techniques measure the deformation by recording the phase difference of the scattered light wave from the test object surface before and after deformation. The measurement results are often presented in the form of fringe patterns; thus, further fringe processing and phase analysis techniques are required. In case of non-interferometry techniques, grid method [27] and digital image correlation (DIC) [28] are used. Non-interferometric techniques determine the surface deformation by comparing the gray intensity changes of the object surface before and after deformation, and generally have less stringent requirements under experimental conditions. Among them, DIC have become most popular in the field of experimental mechanics because of their relatively easier specimen preparation and simple optical arrangement. In this study, DIC is used for the measurement of whole field surface displacement and strain arising in the composite panel.

1.1.5.1 Whole field strain measurement using digital image correlation technique

DIC is a non-interferometric optical technique that has been widely accepted and commonly used as a powerful and flexible tool for the surface deformation measurement in the field of experimental solid mechanics. It directly provides full-field displacements and strains by comparing the digital images of the specimen surface in the un-deformed (or reference) and deformed states respectively [29].

The approach for determining surface deformation using digital image correlation technique has started from the 1980s. It has been developed by a research group ant University of South Carolina. The technique has been improved by many researchers to increase resolution, to improve accuracy and to overcome its draw backs [30].During the past few years, the DIC method has been extensively investigated and significantly improved for reducing computation complexity, achieving high accuracy in deformation measurement and expanding application range.

In principle, DIC is based on pattern matching and numerical computing [29]. In DIC, one of the most commonly used approaches employs random patterns and compares sub-regions

(subsets) from 'deformed' and 'un-deformed' images to obtain a full-field of sensor-plane measurements [31]. In two-dimensional digital image correlation, displacements are directly detected from digital images of the surface of an object. The plain surface of the object is usually observed by a CCD camera with an imaging lens. The images of the surface of the object, one before and another after deformation are recorded, digitized and stored in a computer as digital images. These images are compared to detect displacements by searching a matched point from one image to another. Figure 1.7 shows digital images before and after deformation. Displacement of the subset on the image before deformation is found to be in the image after deformation by searching for the area of same light intensity distribution. Once the location of the subset on the deformed image is found, displacement of the subset can be determined. In order to perform this subset matching process, the specimen surface should have a distinguishable random pattern. So, an artificial random pattern is applied over the surface of the specimen. Figure 1.8 shows a typical random pattern made over surface of a sample by spraying paint.
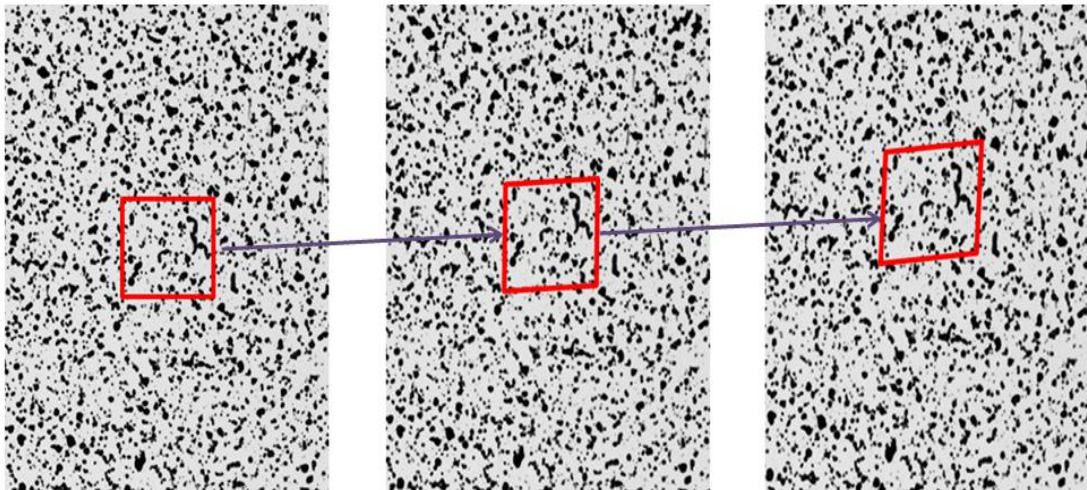
Figure 1.7: Digital images before and after deformation (a) image before deformation (b) and (c) images after deformation.

Figure 1.8: A typical random speckle pattern applied over the specimen.

The basic principle of 2D DIC is the tracking (or matching) of the same points (or pixels) between the two images recorded before and after deformation as schematically illustrated in figure 4. In order to compute the displacements of point P, a square reference subset of $(2M+1) \times (2M+1)$ pixels centered at point P (x_0, y_0) from the reference image is chosen and used to track its corresponding location in the deformed image (See Figure 1.9). The reason why a square subset, rather than an individual pixel, is selected for matching is that the subset comprising a wider variation in gray levels will distinguish itself from other subsets, and can therefore be more uniquely identified in the deformed image [29].
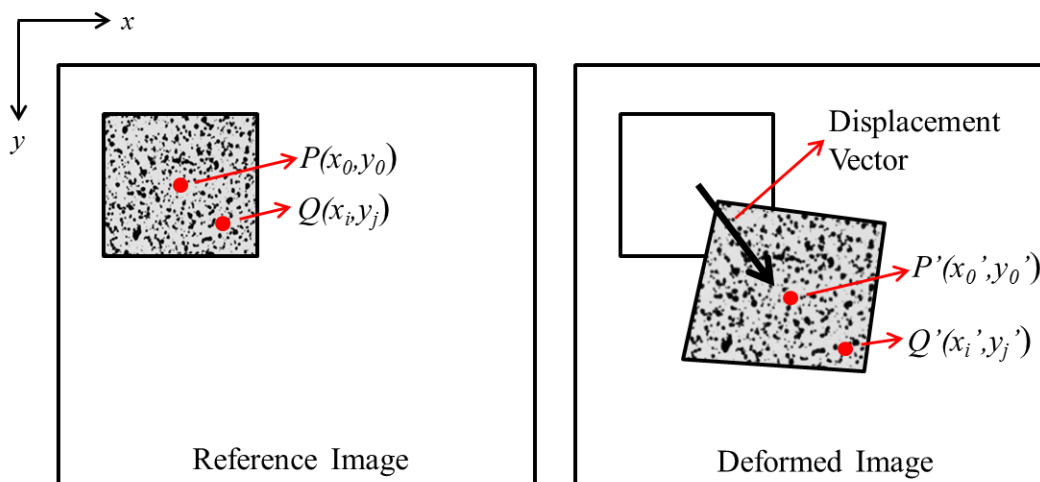
Figure 1.9: Schematic illustration of a reference square subset before deformation and a deformed subset after deformation..

17

In order to evaluate the degree of similarity between the subsets from reference image and the deformed image, different correlation criteria can be used. These criteria can be categorized in to two groups; they are cross-correlation criteria (CC) and sum of squared differences criteria (SSD) as given below.

Cross-correlation (CC)

$$C_{CC} = \sum_{i=-M}^{M} \sum_{j=-M}^{M} \left[f(x_i, y_j) g(x'_i, y'_j) \right] \tag{1}$$

Normalized cross-correlation (NCC)

$$C_{NCC} = \sum_{i=-M}^{M} \sum_{j=-M}^{M} \left[\frac{f(x_i, y_j) g(x'_i, y'_j)}{\overline{f}\ \overline{g}} \right] \tag{2}$$

Zero-normalized cross-correlation (ZNCC)

$$C_{ZNCC} = \sum_{i=-M}^{M} \sum_{j=-M}^{M} \left[\frac{\left[f(x_i, y_j) - f_m \right] \times \left[g(x'_i, y'_j) - g_m \right]}{\Delta f\ \Delta g} \right] \tag{3}$$

Sum of squared differences (SSD)

$$C_{SSD} = \sum_{i=-M}^{M} \sum_{j=-M}^{M} \left[f(x_i, y_j) - g(x'_i, y'_j) \right]^2 \tag{4}$$

Normalized sum of squared differences (NSSD)

$$C_{NSSD} = \sum_{i=-M}^{M} \sum_{j=-M}^{M} \left[\frac{f(x_i, y_j)}{\overline{f}} - \frac{g(x'_i, y'_j)}{\overline{g}} \right]^2 \tag{5}$$

Zero-normalized sum of squared differences (ZNSSD)

$$C_{ZNSSD} = \sum_{i=-M}^{M} \sum_{j=-M}^{M} \left[\frac{f(x_i, y_j) - f_m}{\Delta f} - \frac{g(x'_i, y'_j) - g_m}{\Delta g} \right]^2 \tag{6}$$

Where,

$$f_m = \frac{1}{\left(2M+1\right)^2} \sum_{i=-M}^{M} \sum_{j=-M}^{M} f(x_i, y_j) \tag{7a}$$

$$g_m = \frac{1}{\left(2M+1\right)^2} \sum_{i=-M}^{M} \sum_{j=-M}^{M} g(x'_i, y'_j) \tag{7b}$$

$$\overline{f} = \sqrt{\sum_{i=-M}^{M} \sum_{j=-M}^{M} \left[f(x_i, y_j) \right]^2} \tag{8a}$$

$$\overline{g} = \sqrt{\sum_{i=-M}^{M} \sum_{j=-M}^{M} \left[g(x'_i, y'_j) \right]^2} \tag{8b}$$

$$\Delta f = \sqrt{\sum_{i=-M}^{M} \sum_{j=-M}^{M} \left[f(x_i, y_j) - f_m \right]^2} \tag{9a}$$

$$\Delta g = \sqrt{\sum_{i=-M}^{M} \sum_{j=-M}^{M} \left[g(x'_i, y'_j) - g_m \right]^2} \qquad (9b)$$

$$x' = x + u_0 + \frac{\partial u}{\partial x} dx + \frac{\partial u}{\partial y} dy \qquad (10a)$$

$$y' = y + v_0 + \frac{\partial v}{\partial x} dx + \frac{\partial v}{\partial y} dy \qquad (10b)$$

$f(x, y)$ and $g(x', y')$ represent the gray levels of reference and deformed images, respectively; and (x, y) and (x', y') are the co-ordinates of a point in the subset before and after deformation respectively.

The matching procedure is completed through searching the peak position of the distribution of correlation coefficient. Once the correlation coefficient extremum is detected, the position of the deformed subset is determined. The differences in the positions of the reference subset center and the deformed subset center yield the in-plane displacement vector at point P, as illustrated in Figure 1.9.

Once the maximum of this correlation coefficient is detected, the position of the deformed subset is determined. Then, in-plane displacement vector at point P can be calculated using the difference in the positions of the reference subset center and the deformed subset center [29].

The discrete nature of the digital image enables computation of the integer displacements with 1 pixel accuracy. Certain sub-pixel registration algorithms can be used to further improve displacement measurement accuracy. Generally, to achieve sub-pixel accuracy, the implementation of 2D DIC comprises of two consecutive steps, namely initial deformation estimation and sub-pixel displacement measurement. 2D DIC method normally requires an accurate initial guess of the deformation before achieving sub-pixel accuracy. For e.g., for the most commonly used iterative spatial cross-correlation algorithm (e.g. the Newton Raphson method) only converges when an accurate initial guess is provided [29]. Techniques are therefore required to achieve a reliable initial guess of deformation. Inspired by the nested coarse–fine algorithm presented by Zhan get al. [32] that can provide an initial guess for each calculation point, a technique is presented by Pan et al. [29] to achieve a reliable initial guess for the Newton Raphson method for these cases. Slightly different from Zhang's work, this technique only provides the initial guess of the first calculation point. Alternatively, benefiting from the extraordinary ability of its global optimum, the genetic algorithm can also be used as an automatic technique for determining the initial guess of the

first calculation point. However, the genetic algorithm normally costs a lot of computation time to converge to the global extremum [29].

In many tasks of experimental solid mechanics such as mechanical testing of material and structure stress analysis, full-field strain distributions are more important and desirable. But, less work has been devoted on the reliable estimation of strain fields. Presumably, this can be attributed to the fact that the displacement gradients (i.e. strains) can be directly calculated using the Newton Raphson or genetic algorithm. Alternatively, the strains can be computed as a numerical differentiation process of the estimated displacement. It should be noted that the error of estimated displacement gradients using the Newton-Raphson or genetic method normally limits its use only to local strains greater than approximately 0.010. Although the relationship between the strain and displacement can be described as a numerical differentiation process in mathematical theory, unfortunately, the numerical differentiation is considered as an unstable and risky operation, because it can amplify the noise contained in the computed displacement. Therefore, the resultant strains are unreliable if they are calculated by directly differentiating the estimated noisy displacements [29]. So, the accuracy of strain estimation can be improved by smoothing the computed displacement fields first and subsequently differentiating them to calculate strains. Based on these considerations, a technique is utilized by Shi et al. [33] to compute the thermal deformation of electronic packaging. In addition, thin plate spline smoothing technique and generalized cross validation technique were introduced by Wang et al. [34] to remove the noises contained in displacement fields. However, smoothing noisy discrete data using the penalty finite element method or thin plates spline is quite cumbersome. More recently, Xiang et al. [35] used the moving least-squares (MLS) method to smooth the displacement field followed by a numerical differentiation of the smoothed displacement field to get the strain fields. The more practical technique for strain estimation is the point wise local least-squares fitting technique used and advocated by Pan et al [36]. The technique is used by them with a simpler and more effective data processing technique for the calculation of strains for the points located at the image boundary, hole, cracks and the other discontinuity areas.

Since two dimensional digital image correlation requires predominantly in-plane displacements and strains, relatively small out of plane motion will change the magnification and introduce errors in the measured in-plane displacement. So, 2D-DIC is applicable only for planar objects that exhibit little or no out-of-plane displacement and cases where the recording camera can be set perpendicular to the object surface [30]. In

actual practice, it may not be possible to avoid the out-of-plane deformation. To overcome this fundamental limitation, three-dimensional (3D) DIC method is developed which uses a stereo vision system employing two or more cameras to accurately measure the full three-dimensional shape and deformation of a curved or planar object, even when the object undergoes large out-of-plane rotation and displacement [28-29, 31]. Whereas two-dimensional (2D) DIC uses a single imaging camera, the sensor plane of which is kept parallel to the surface of planar object. Figure 1.10 shows a typical image acquisition system arrangement for 3D DIC. Figure 1.11 shows whole field strain and displacement plots for a composite panel with multiple holes obtained using 3D DIC.

1.2 Literature Review

1.2.1 Strength prediction and damage study of composite laminates with holes

Behavior of composite panels with holes or cut-outs has attracted attention of number of researchers. Toubal et al. [24] investigated strain field of a composite plate in the presence of stress concentration due to circular hole in the panel. A non-contact method, namely electronic speckle pattern interferometer (ESPI) clearly revealed the strain concentrations near the singularity. Failure in fiber reinforced laminated composite structures containing discontinuities, such as holes or notches has been one of the key areas which has interested many researchers. Many studies have been carried out by various researchers to predict the failure strengths of composite laminates containing stress concentrations such as induced by circular holes or cutouts. Kazemahvazi et al. [37] have presented the study about the tensile strength of unidirectional glass/epoxy laminates with multiple holes. Different types of hole patterns were investigated experimentally. It is concluded that the failure mode changes with changing hole pattern and hole density. Dan-Jumbo et al. [38] have carried out a study on the strength prediction in graphite/epoxy laminate having multiple holes. Both experiment and finite element based study has been carried out to compare the strength of laminates having different hole patterns. They have found that strength of laminate is highest for two inline holes and lowest for four holes in diamond array pattern. Also they further observed that presence of more holes in the loading direction reduces the stress concentration factor (SCF) in the panel. Manoharan et al. [39] have done a study on open cut out panel under compressive load. Different orientations of fibers are examined for specimen with and without cutout. They have concluded that maximum load bearing capacity decreases as the cut-out size increases.
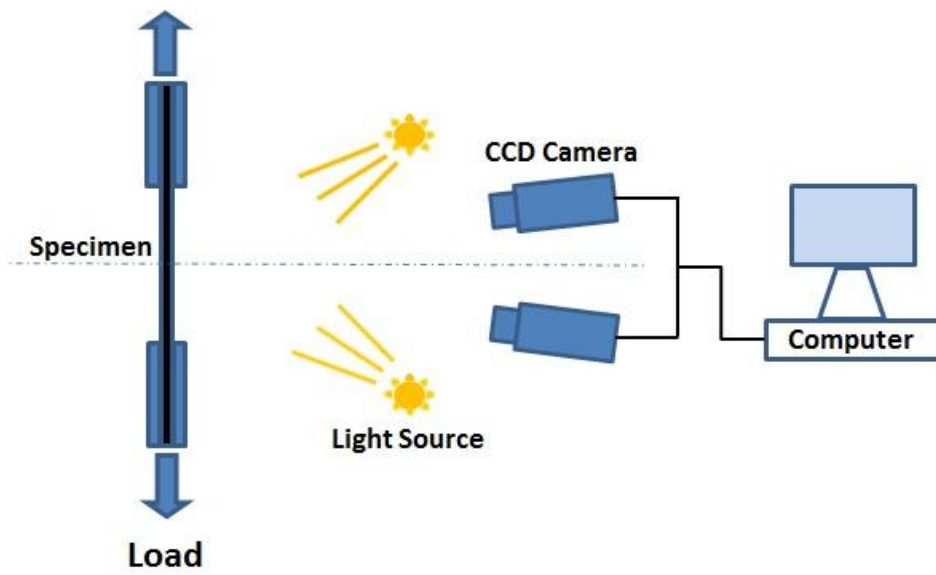
Figure 1.10: Typical image acquisition system for 3D DIC system
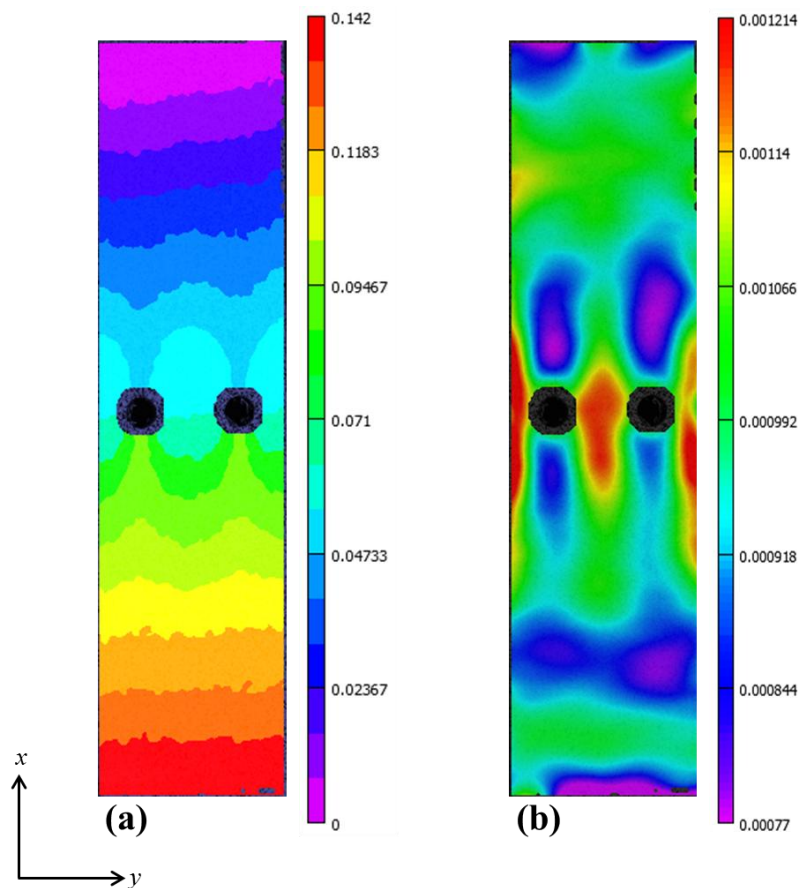
Figure 1.11: (a) Whole field ε_{xx} strain distribution in a CFRP panel having two holes (b) Whole field u displacement distribution in a CFRP panel having two holes

Progressive failure analysis which is performed to predict the damage propagation and strength of composite materials consists of stress or strain analysis, damage prediction and damage modeling. Fist, stresses or strains are estimated for each element in the principal material direction of the laminate under prescribed loading condition. Damage prediction in composite laminates is very complicated mainly due to the presence of different failure modes or combination of them. It is performed by substituting the element stresses or strains in to a suitable failure theory. There are number of failure theories available for damage prediction [9-22, 40-42]. Once the damage is detected in any of the elements, damage modeling needs to be done using any of the various techniques that have been developed for modeling the damage. It is done for mimicking loss in load carrying capacity of the failed element. Chang and Chang [15] have presented a progressive damage model (PDM) for notched laminated composites subjected to tensile loading. Their model can assess damage in laminates with different ply orientations and predict ultimate strength of notched laminates. Damage modeling is done with the help of material property degradation method (MPDM). Numerical results are validated with experimental data on laminates containing open circular hole. But this study is carried out for panel with single cut out. Yang and Chow [43] have carried out progressive damage analysis of unidirectional graphite/epoxy composites containing a circular cut-out. Experimental and finite element results are presented to describe the anisotropic state of stress, strain and the damage of composite panel containing circular hole subjected to tensile load. Their study revealed that redistribution of stresses and strains due to damage accumulation determine the subsequent path of damage development and also the load carrying capacity of composite structure. They used Moiré interferometry technique to study the deformation in the composite laminates. But in Moiré interferometry, optics is quiet involved and it is very sensitive to vibration. Progressive failure analysis of laminated composite plates under transverse loading has been carried out in linear and elastic range by Pal and Ray [44]. Stiffness degradation is implemented for the damage modeling. The results in terms of first ply failure load obtained in the study are compared with the results already available in the published literature. Hallet and Wisnom [3] have performed an experimental investigation of progressive damage on notched specimen under tensile load. It is observed that failure mechanism varied with both layup and specimen size. Lapczyk and Hurtado [45] have presented a study on the progressive damage of fiber reinforced materials. Four different failure modes are considered and modeled separately. Damage initiation is predicted using Hashin's failure criteria and damage evolution is carried out using a separate law. The damage evolution law is based on fracture energy dissipation happening during damage

process. A comparative study of open hole laminates made of glass and carbon fiber reinforced composite materials has been performed by O'Higgins et al. [46]. Experimental study has been carried out and non-destructive tests are conducted to map the damage progression. The damage progression and failure mechanism for these two materials is found to be very similar. Tay et al. [47] have carried out a study on the progressive failure analysis of composite laminates. Their study is based on a novel method called element failure method (EFM) for damage modeling. Results for notched as well as pin loaded laminates are shown and compared with the experimental behavior. Zhang and Zhao [48] have developed a PDM for fiber reinforced composite laminates containing a hole. They have employed micromechanical model to evaluate the failure criteria at the micro level.

1.2.2 Damage study of mechanically fastened joints in composite laminates

Hassan et al. [49] have conducted a 3D finite element analysis (FEA) based study of single and multi-bolted joints in composites to determine the failure process, ultimate load and the load distribution among the fasteners. Tsai Wu polynomial failure criterion has been applied for failure detection. Camanho and Mathews [40] have developed a 3D finite element based PDM for mechanically fastened joint in composite laminates. Hashin failure criteria is used to detect the damage and stiffness degradation method is implemented for progressive damage modeling. Aktas et al. [50] have investigated failure strength and failure mode of a mechanically fastened carbon/epoxy composite plate of arbitrary orientation. The failure load and the failure mode are analyzed numerically and experimentally. Failure load and the failure mode are predicted by means of Tsai-Hill and fiber tensile-compressive failure criteria. Ireman [51] has conducted a study which involves strength prediction in composite laminates containing bolt holes and open holes. The study covers both 2D and 3D finite element analyses and experiments are carried out to determine criteria parameters and to validate the analysis methods. Different failure criteria, including the Point Stress Criterion and the Damage Zone Criterion have been used to predict the strength of test specimens subjected to complex loading conditions. Tserpes et al. [52] has conducted a parametric finite element analysis to investigate the effect of failure criteria and material property degradation rules on the tensile behavior and strength of bolted joints in graphite/epoxy composite laminates. Load – displacement curves and failure loads predicted for a single-lap single-bolt joint are compared with experimental data for different joint geometries and laminate stacking sequences. They have found out that the predicted failure load is significantly influenced by the combination of failure criteria and degradation rules used. A

combination of failure criteria and material property degradation rules that leads to accurate strength prediction has been proposed.

Kermanidis et al. [41] has developed a 3D progressive damage model in order to simulate the damage accumulation of bolted single-lap composite joints under in-plane tensile loading. Their model is capable of predicting the residual strength and residual stiffness of laminates with arbitrary lay-ups, geometries and bolt positions. Hashin's failure criteria together with a set of appropriate degradation rules is used for developing the progressive damage model. McCarthy et al. [42] have developed a PDM for multiple bolted double lap composite joints. The model is validated by comparing load–displacement characteristics and surface strains to experimental results. It is shown that bolt-hole clearance can cause major changes in the load distribution as well as damage mechanisms in the joint. Strength analysis of mechanically fastened joints layered composite structures is performed by Ilić [53]. The failure of mechanically fastened joint is determined by combining the Chang-Scott-Springer model of the characteristic curve and the Tsai-Wu initial failure criterion. The numerical results are compared to author's own experimental results and good agreement is obtained. Kishore et al. [54] have conducted a study to obtain failure loads and failure modes of multi-pin joints in uni-directional glass fiber/epoxy composite laminates by finite element analysis. Tsai-Wu failure criteria associated with material property degradation is used in their study to predict failure load and determine failure modes. Finite element analysis results were validated by comparing with experimental results. Their study proves that it is very important to consider the effect of of variation in pitch-to-diameter ratio, width-to-diameter and edge-to-diameter ratios. Pisano and Fuschi [55] have proposed a numerical approach for statically loaded pinned-joint in orthotropic laminates under in plane stress conditions. The study is based on the application of limit analysis theory. Upper and lower bounds to the joint collapse load are evaluated in the study. An experimental and numerical analysis has been carried out by Aktas [56] to determine failure and failure mode of glass/epoxy composite laminates with one and two serial pinned joints. Yamada Sun failure criterion is used for the failure detection. An analysis of multi-pin joints in composite laminates has been carried out by Pisano et al. [57] for the prediction of failure mode. The study is based on the application of limit analysis theory. Comparison between the numerically predicted failure modes and the experimentally detected ones shows that the proposed methodology furnishes reliable information.

1.3   Scope and Motivation

Failure in fiber reinforced laminated composite structures containing discontinuities, such as holes or notches has been one of the key areas which has interested many researchers. Most of the reported work involves progressive failure analysis of panel with single open hole. But many structures contain multiple holes in them for various purposes like joints, electrical connections etc,. Thus, there is a need to understand the failure mechanism and also to predict the strength of composite panel with multiple interacting holes.

One such extension of multiple hole is joining of composite panels using pin joint. In the case of pin joints in composite laminates, the presence of unknown contact stresses and contact region between the fastener and the laminate make the analysis more complex than that of a traction-free hole. Understanding the mechanical and damage behavior of pin joint composite panel under loading is very important towards their structural applications. The accurate prediction of the material behavior along the hole edge is essential for reliable strength evaluation and failure prediction. Also prediction of failure strength and failure mechanism of multi-pin joints in composite laminates is very much required for a damage tolerant design.

1.4   Thesis layout

Chapter 1 explains briefly about composite materials, progressive failure analysis of composite laminates, various experimental techniques used to study the mechanical behavior of composites. A brief introduction to DIC technique is presented followed by literature review of strength prediction and damage study of composite laminates with holes as well as of mechanically fastened joints in composite laminates. It also briefly explains about scope and motivation for the thesis.

Chapter 2 deals with the development of a progressive damage model that can be applied to composite panels with multiple interacting open circular holes. A finite element model is developed dealing with the implementation of various aspects as part of progressive damage model. It also explains about specimen preparation and DIC experimental procedure. Finally validation of numerical results is carried out using the DIC results.

Chapter 3 deals with the development of progressive damage model for multi-pin joints in composite laminate. It explains about development of finite element model for implementation of progressive damage model. Also DIC experiments are done for qualitative comparison and the FEA prediction is compared against them.

Chapter 4 is the conclusion and recommendation for the future work.

Chapter 2

Progressive Damage Model for Composite Laminate with Multiple Interacting Holes

2.1   Introduction

In this chapter, 3D finite element based progressive damage model (PDM) is presented for unidirectional CFRP laminates having two holes in different configurations subjected to tensile loading. The developed model is suitable for predicting failure and post failure behavior of fiber reinforced composite materials. The material is assumed to behave as linear elastic until final failure. The stress values are estimated using 3D finite element analysis and damage prediction is done using Hashin's failure criterion for unidirectional composite laminates [14]. Damage modeling is accomplished using material property degradation method (MPDM) [42-43, 45].

Digital image correlation (DIC) experiment is carried out to perform whole field strain analysis of CFRP panel with different hole configurations. Whole field surface strain and displacement from finite element prediction are compared with DIC results for validation of the finite element model. A progressive damage model is developed which can predict the onset of damage, damage progression and the post failure response. Load-deflection behavior as well as path of damage progression is predicted by both PDM simulation and experiment. They are found to be in good agreement thereby confirming the accuracy of PDM implementation.

The longitudinal as well as transvers spacing between hole affect greatly on the behavior of panel with multiple holes. The maximum stress value in a panel with multiple holes changes

with change in spacing. The spacing thereby influences the damage process too. Effect of spacing between the holes on stress concentration factor (SCF) is also further investigated in this chapter.

2.2   Problem description

In this study, unidirectional carbon/epoxy composite laminates having two holes of different configurations are considered. The panel is of $[0^o]_4$ configuration. The length (L), width (W) and the thickness (t) of the panel are 150 mm, 36 mm and 1.2 mm respectively. Diameter (D) of the hole is 6 mm. Composite laminates with three different hole configurations as shown in Figure 2.1 are analyzed as part of this work. Configuration 2HL contains two holes in the longitudinal direction whereas configuration 2HT contains two holes in the transverse direction. Configuration 2HD is having two holes placed in diagonal pattern. Spacing (SL, ST) in longitudinal/transverse direction between the two holes for all the configurations is 19 mm. An in plane incremental tensile load is applied to the composite laminates and the fibers are aligned along the loading direction.
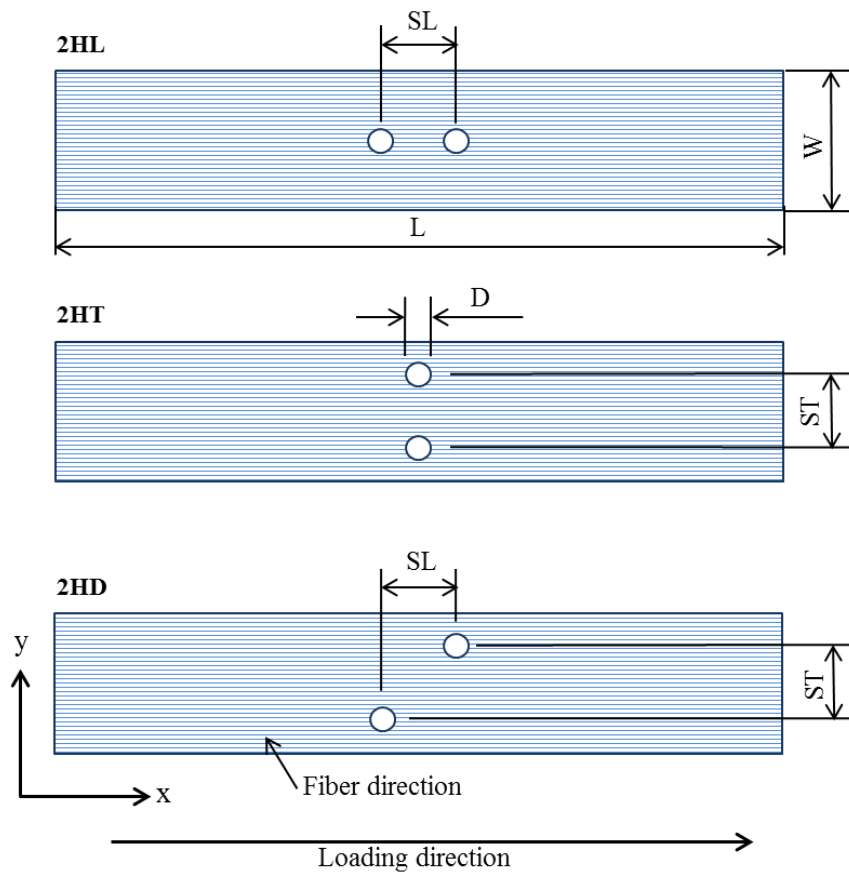
Figure 2.1: Different hole configurations studied

2.3 Experimental Analysis involving DIC

As mentioned in section 2.2, three type of specimen are considered for this study. Composite specimens are prepared as per the dimensions mentioned and experiments are carried out involving DIC. Experiment results are used for the validation of finite element model an also of the progressive damage model.

2.3.1 Specimen preparation

Composite laminates are fabricated by hand layup technique with unidirectional carbon fiber mat of 200 gsm (Goldbond®). Matrix material used is a mixture of epoxy resin LY556 with hardener HY951 in the ratio of 10:1 by weight. A high precision weighing machine is used to weigh the resin and hardener. The resin and hardener are taken and mixed thoroughly in the ratio of 10:1 without formation of bubbles. Formation of bubbles could cause formation of air voids in the finished casting. A flat Perspex sheet is used as mold for the fabrication. The perspex sheet is cleaned with isopropyl alcohol. Mylar sheet is used to cover the mold for obtaining better surface finish. Appropriate quantity of resin-hardener mixture is poured over the mold covered with Mylar sheet and is spread over the mold area using brush. First layer of carbon fiber is then placed over the mold in appropriate direction and teflon roller is rolled over the carbon fiber mat in the direction of fiber in order to squeeze out the excess resin. Successive layers of carbon fiber in required direction are placed and resin hardener mixture is poured over each layer and the same process is repeated. Another layer of mylar film is finally placed on top of the laminates and squeezed firmly with roller so as to remove the entrapped air. The composite laminate is then allowed to cure at room temperature for 24 hours. Specimens are cut from laminate to appropriate dimensions using abrasive cutter mounted on a hand-held saw. Specimens are machined to their exact dimensions using milling machine with carbide coated end mills at a speed of 80 rpm. Wooden backing plates are used to avoid edge delamination. Holes in the laminates are drilled in radial drilling machine with carbide coated drill bit of required diameter at a speed of 250 rpm. Wooden backing plate is used at the bottom of specimen to avoid hole-exit delamination induced due to drilling operation. Aluminium tabs of required dimension are bonded to the test specimen using AV138/HV998 adhesives after roughening of bonding surfaces using sand paper followed by cleaning of surface with isopropyl alcohol. Tabs are provided at the end of the specimen for obtaining a better grip and to avoid damage while specimen is loaded in the fatigue testing machine. Figure 2.2 illustrates the various steps involved in specimen preparation.

Figure 2.2: Different steps in CFRP specimen preparation

To perform DIC experiment, random speckle patterns are created over the specimen surface. DIC speckle pattern is applied by using acrylic paints of black and white color. First the specimen surface is cleaned using isopropyl alcohol. Golden® acrylic paint of titanium white color is applied over the specimen surface using air brush. Only one layer of white paint is applied to avoid changing the shape of the surface and increasing shear effect due to the higher thickness of paint coating. The white paint is allowed to dry for 1 hour. Golden® acrylic paint of carbon black color is applied over the specimen surface (white color painted) in a random fashion using an air brush to get a random speckle pattern. The air brush used is having a nozzle diameter of 0.5 mm. Based on observation of pattern made at different air pressures, an air pressure of 0.15 MPa is chosen at which adequate size and density of the black dots are obtained. For one set of specimen, a different plate preparation technique is used in order to avoid losing important DIC displacement data at and near the edge of the hole as explained in Ref. [58]. Losing of important DIC displacement data at and near the edge of the hole is because DIC software's correlation algorithm is not able to compare a group of pixels that don't have any neighboring pixels [58]. In order to avoid this, the holes are filled with clay before application of speckle pattern. Continuity of speckle pattern is obtained near the edges of clay filled holes. By clay filling of the holes, displacements and strain data near the hole edges is obtained without affecting the structural performance of the CFRP panel. Figure 2.3 shows the DIC samples for all the hole configurations with speckle pattern.

2.3.2   Experimental test procedure

The experimental setup used for present study is shown in Figure 2.4. Experiments are carried out at room temperature using an MTS Landmark® servo-hydraulic cyclic test machine of 100 kN capacity. Specimen is fixed into hydraulic wedge grips with appropriate grip pressure and aligned properly. A 3D-DIC system (supplied by Correlated Solutions, Inc.) is used which consists of two 8-bit Grasshopper® CCD Cameras (POINTGREY - GRAS-50S5M-C) with a resolution of 2448 x 2048 pixels, coupled with Schneider Xenoplan lenses of 35 mm focal length. Both cameras are mounted on a tripod having inbuilt spirit level to ensure horizontal level. The cameras are properly aligned with respect to the specimen. Two white light emitting diode light sources (30 W capacities) are provided on both sides of the cameras for illumination of the specimen surface. The positions of the light sources are adjusted to maintain proper of illumination without causing over saturation of pixels in the captured images. Cameras are then connected to mobile workstation laptop using a grabbing card and calibration is done for camera position and

orientation using a set of grid plates. Vic-Snap 2009 software is used for image grabbing and calibration. Images are grabbed at predefined interval of time while applying uniaxial tensile load. The test is done at a cross head speed of 1 mm/minute. Load and displacement values are stored corresponding to every image being grabbed using a data acquisition card which interfaces image grabbing system with the MTS controller system. The test is aborted when the final failure is reached. Figure 2.5 shows the DIC images which show the final failure of the specimens.

Full field in-plane displacement fields need to be estimated from the captured images. It is performed by searching for the maximum correlation between small zones of the specimen (subsets) in the unreformed (reference) and deformed images. The estimated displacement data is smoothed and then numerical differentiation of them is carried out to obtain the full field strain field all over the specimen surface. In this study, VIC-3D 2010 software from Correlated Solutions is used for estimating displacement and strain fields.

(a)   (b)   (c)
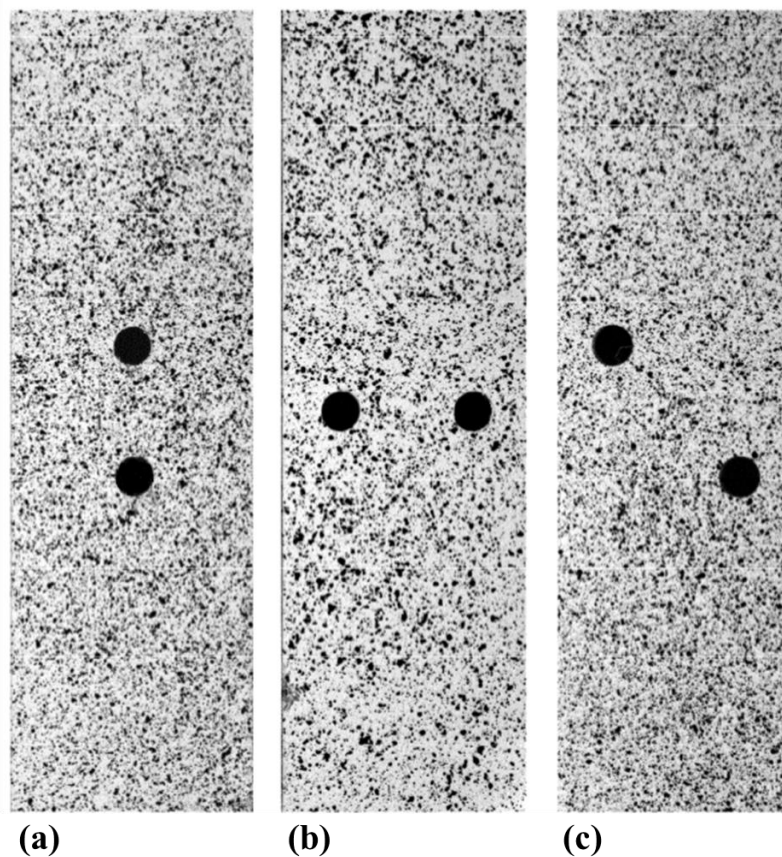
Figure 2.3: Specimen of different hole configurations applied with speckle pattern (a) 2HL (b) 2HT (c) 2HD
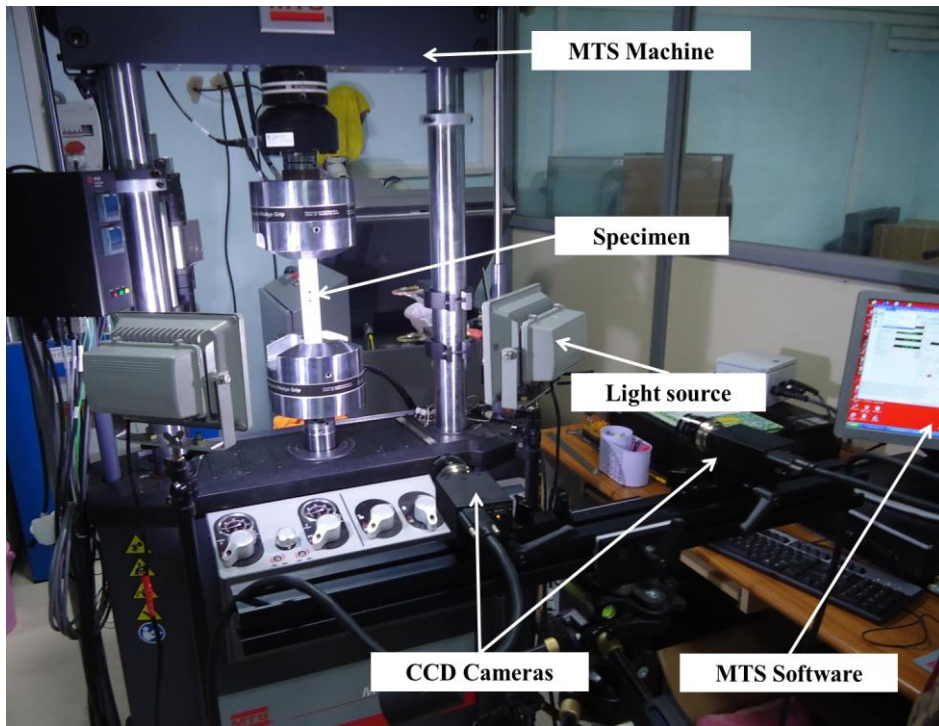
Figure 2.4: Experimental setup

| (a) | (b) | (c) |
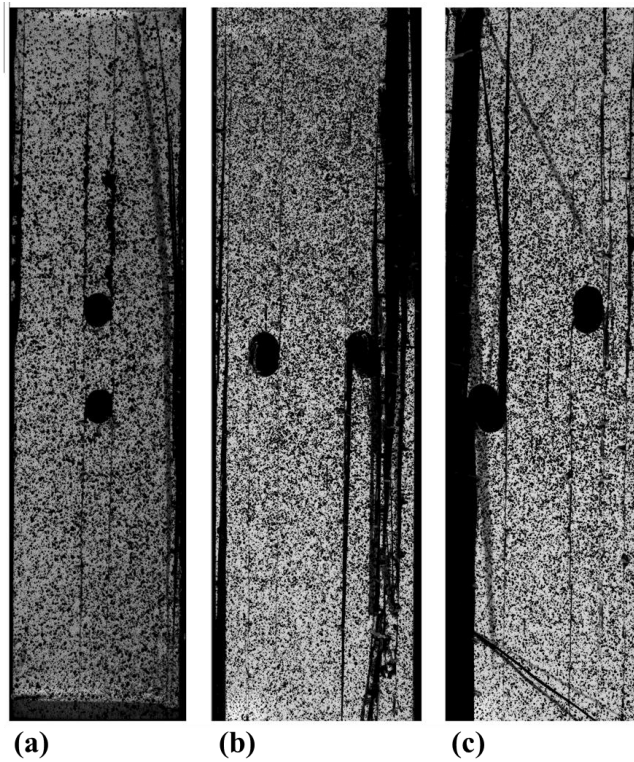
Figure 2.5: Images showing the final failure of panels with different hole configurations
(a) 2HL (b) 2HT (c) 2HD

2.3.3 Material characterization of carbon/epoxy composite laminates

Material properties of the carbon/epoxy composite laminates are determined at room temperature using DIC as given in Ref. [59-60] and they are as per ASTM standards. Tensile tests are performed as per ASTM standard D-3039 [61]. Unidirectional (0^0) specimens are tested to evaluate longitudinal properties. Ten images per second are grabbed at a displacement control rate of 2 mm/min. Unidirectional (90^0) specimens are tested to evaluate transverse properties. Ten images per second are grabbed at displacement control rate of 1 mm/min. Compression tests are performed as per ASTM D-3410 [62] standard. Unidirectional (0^0 & 90^0) specimens are tested to evaluate strength parameters under compressive load. Ten images per second are grabbed at a displacement control rate of 1.125 mm/min. Shear tests are performed as per ASTM D-3518 [63] standard. The ($\pm45^0$) tensile specimens are tested which provides an indirect means to evaluate in-plane shear modulus and shear strengths parameters. Ten images per second are grabbed at a displacement control rate of 1 mm/min [60]. Strain values for tensile and shear test are obtained from DIC. Young's moduli in longitudinal and transverse direction are calculated from initial slope of stress–strain curves. In-plane shear modulus is obtained by initial slope of shear stress–shear strain curve. Procedure followed for finding shear stress, shear strength and shear strain is as per ASTM D-3518 and is explained in Appendix A. The longitudinal and transverse tensile as well as compressive strength parameters are obtained by dividing the failure load to the cross-sectional area of the respective specimens. For estimating out of plane properties, procedure is adopted from Ref. [64] and it is briefly outlined in Appendix B. The material properties of Carbon/Epoxy composite laminate obtained from the above mentioned tests are given in Table 1. Burn out test is performed to find out the volume fraction of the laminates. A volume fraction of 35% is obtained from the test.

2.4 Finite Element Model

This section focuses on the development of 3D finite element model of the panel. It is done using ANSYS 13 which is a commercially available finite element package. Initially, two dimensional areas is created as per the model dimensions and meshed with mesh 200 element having 8 nodes. Later, all the areas are extruded in thickness direction to generate volume. The area mesh is swept in the thickness direction throughout the volume to generate 3D elements. The mesh sweeping is done using SOLID 186 element, which is a 20 noded brick element. The entire model contains a mapped mesh configuration. The mesh pattern surrounding the hole is kept very fine in order to capture the high stress gradient around it. The mesh around the circular hole has a total of 9216 elements (96

35

circumferential; 12 Radial; 8 elements through the thickness). The number of elements along circumferential direction is chosen based on the mesh convergence study performed. Away from the hole, a coarser mesh has been adopted in order to reduce the total degrees of freedom so that the computational time can be minimized. Each layup contains one element in thickness direction. For all the cases, full models are analyzed since symmetry is lost after the damage development. Orthotropic material properties from DIC tests [59-60] are applied to the finite element model. Figure 2.6 shows the finite element model of panels having different hole configurations. The zoomed view of the finite element model around the hole is shown in Figure 2.7.

Table 2.1: Material properties of the Carbon/Epoxy laminate

Material properties	
Longitudinal modulus , E_{xx} (GPa)	81.9
Transverse modulus, $E_{yy} = E_{zz}$ (GPa)	6.15
Shear moduli, $G_{xy} = G_{xz}$ (GPa)	2.77
Shear modulus, G_{yz} (GPa)	2.2
Poisson's ratio (v_{xy})	0.34
Poisson's ratio (v_{xz})	0.34
Poisson's ratio (v_{yz})	0.3
Longitudinal tensile strength, X_T (MPa)	1300
Transverse tensile strength, Y_T (MPa)	22.97
Longitudinal compressive strength, X_C (MPa)	640
Transverse compressive strength, Y_C (MPa)	93.2
Shear strength, $S_{xy} = S_{xz}$ (MPa)	45.1
Shear strength, S_{yz} (MPa)	22.55

2.4.1   Boundary conditions

The boundary condition applied to the finite models is discussed below. The degree of freedom along x-direction is constrained on bottom face of the laminate. In addition, nodes along $z = 0$ on the bottom face are constrained in z-direction. Also nodes along $y = 0$ on the bottom face are constrained in y-direction. The degree of freedom along x-direction of all the nodes in the top face of the specimen is coupled together and displacement in x-direction (u) is applied at the master node which is located at the center of that face.
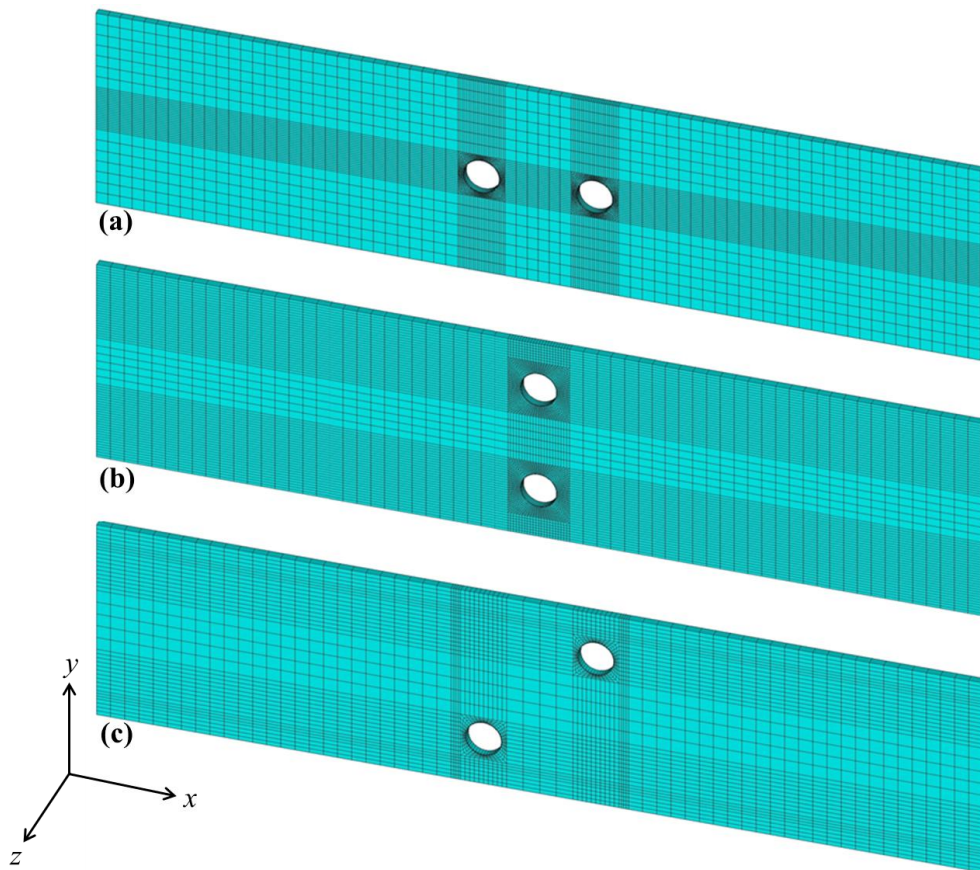
**Figure 2.6: Finite element model for panels having different hole configurations
(a) 2HL (b) 2HT (c) 2HD**
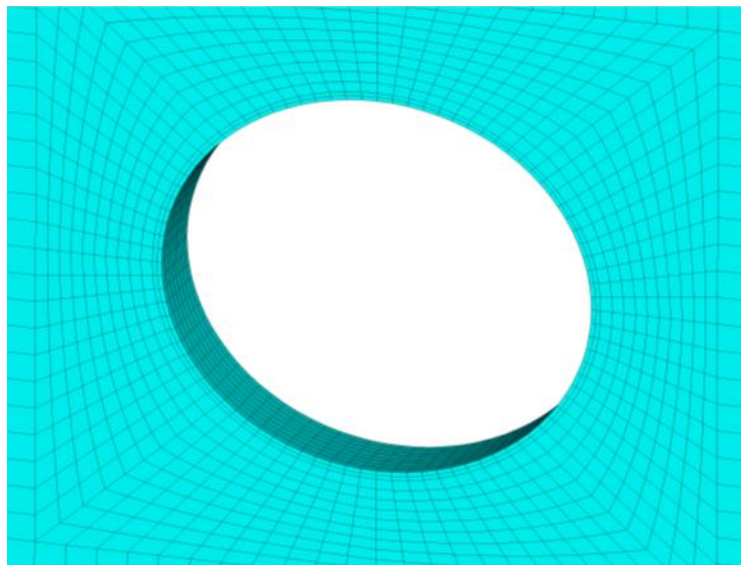
Figure 2.7: Zoomed view of the finite element model around the hole

2.5   Finite Element Model Validation

To validate the finite element model, whole field surface strains from FEA is compared with those from DIC experiment. This is done to make sure that the load, boundary conditions and mesh requirement pertaining to the finite element models are accurate or adequate enough to replicate the experimental behavior of panel having different hole configurations. Also the material property definition can be verified. Figure 2.8 shows the whole field ε_{xx} strain distribution obtained from both DIC and FEA for the panel with 2HL configuration. Figure 2.9 shows the line variation of ε_{xx} from hole edge to free edge of the specimen (see Figure 2.8) at a load of 3.53 kN. The finite element results under-predicts the strain value compared to DIC but the trend of increasing strain towards the hole edge is captured by both FEA and DIC. Figure 2.10 shows a similar comparative plot for 2HT configuration at a load of 3.405 kN. Figure 2.11 shows the variation of ε_{xx} along a line shown in Figure 2.10. Similarly, Figures 2.12 and 2.13 show the whole field ε_{xx} surface strain distribution and line variation of ε_{xx} surface strain both from FEA and DIC for the panel with 2HD configuration at a load of 3.5 kN. It can be observed that a close quantitative agreement exists between FEA and DIC strain field. For all the configurations, whole field displacement field is also shown for better appreciation (see Figure 2.14). Comparison is done between FEA and DIC results for all the three hole configurations. As can be observed, remarkably good agreement exists between FEA and DIC displacement values thereby confirming the accuracy of finite element model.

2.6   Progressive Damage Model

Progressive damage modeling is performed based on the assumption that material shows linear elastic behavior until final failure. There are three major steps involved in PDM and they are stress analysis, damage prediction and damage modeling. Stress analysis is done by FEM involving ANSYS 13 commercial finite element package. In this step, stresses are estimated for each element in the principal material direction of the laminate. Figure 2.15 shows the stress distribution and the location of maximum stress in panels with different hole configurations. Damage prediction in composite laminates is very complicated mainly due to the presence of different failure modes or combination of them. There are number of failure criterion available for damage prediction [8-22, 40-42]. In this study Hashin's failure criterion [14] is used and it is a stress based failure criterion generally employed for damage prediction.
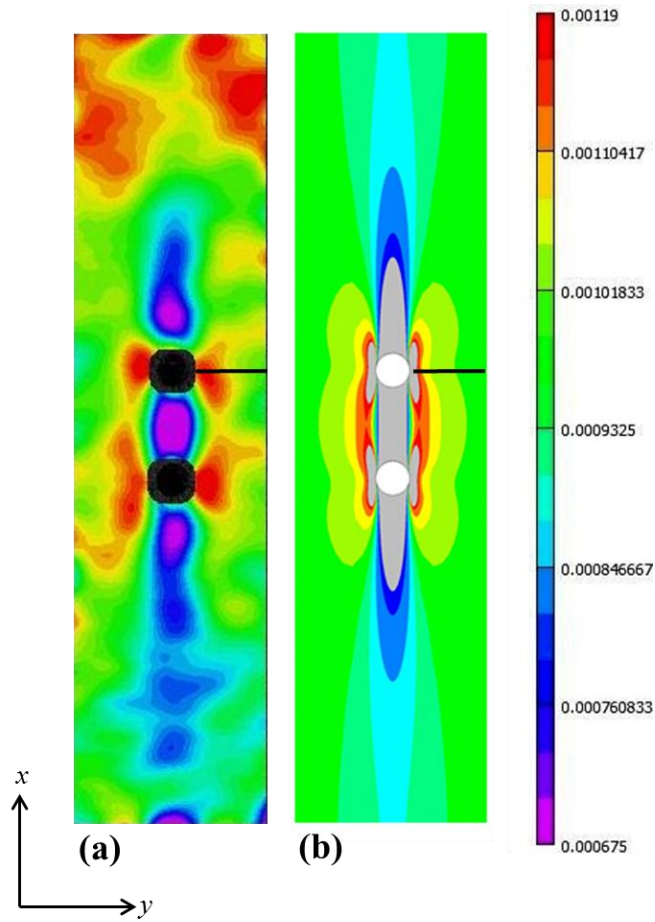
Figure 2.8: Whole field ε_{xx} strain distribution in the panel having 2HL configuration at 3.53 kN load (a) DIC (b) FEA
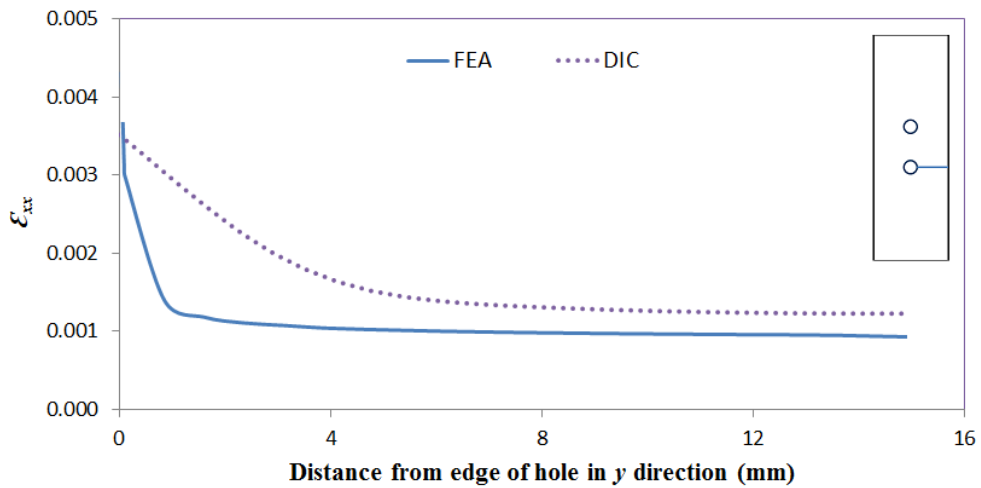
Figure 2.9: ε_{xx} strain variation from hole edge to free edge for the panel having 2HL configuration at 3.53 kN load

39
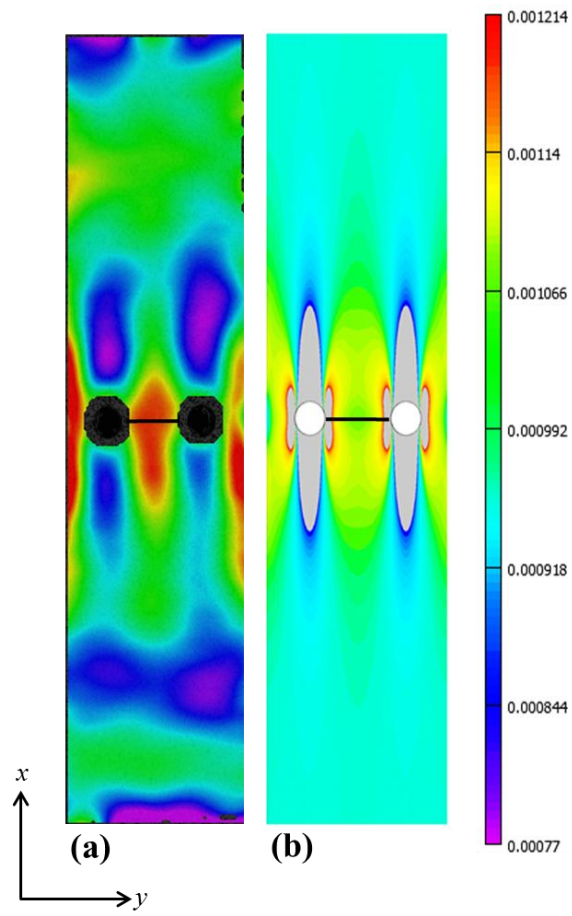
Figure 2.10: Whole field ε_{xx} strain distribution in the panel having 2HT configuration at 3.405 kN load (a) DIC (b) FEA
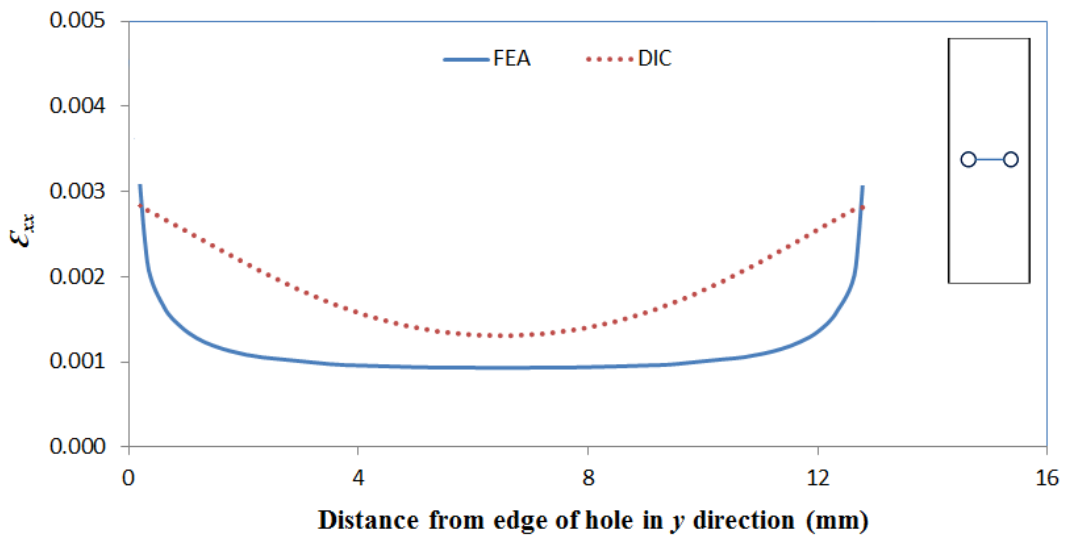
Figure 2.11: ε_{xx} strain variation along a line in 2HT panel configuration at 3.405 kN load
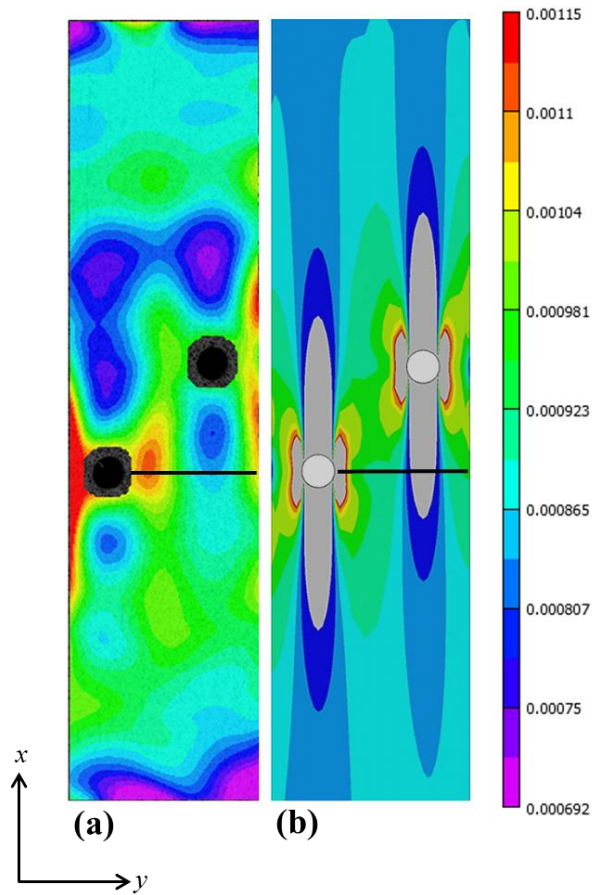
Figure: 2.12 Whole field ε_{xx} strain distribution in the panel having 2HD configuration at 3.5 kN load (a) DIC (b) FEA
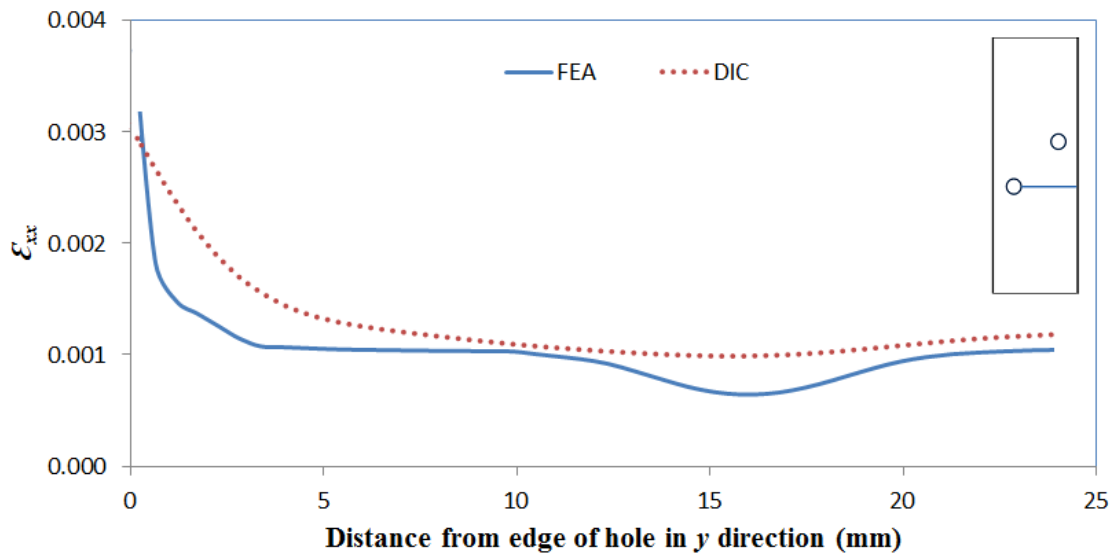
Figure 2.13: ε_{xx} strain variation from hole edge to free edge of the panel with 2HD configuration at 3.5 kN load
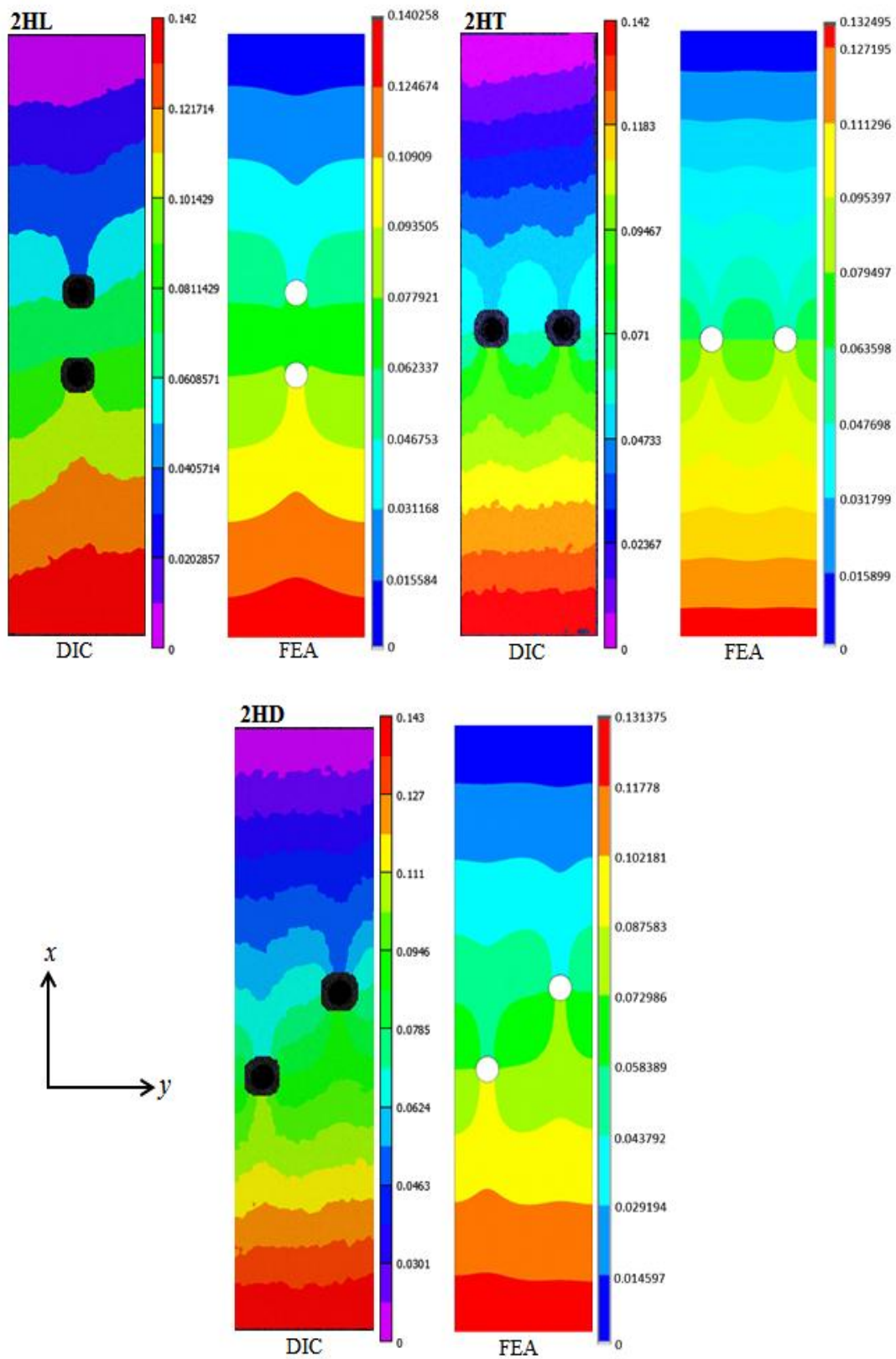
Figure 2.14: Whole field *u*-displacement for panel with different hole configurations
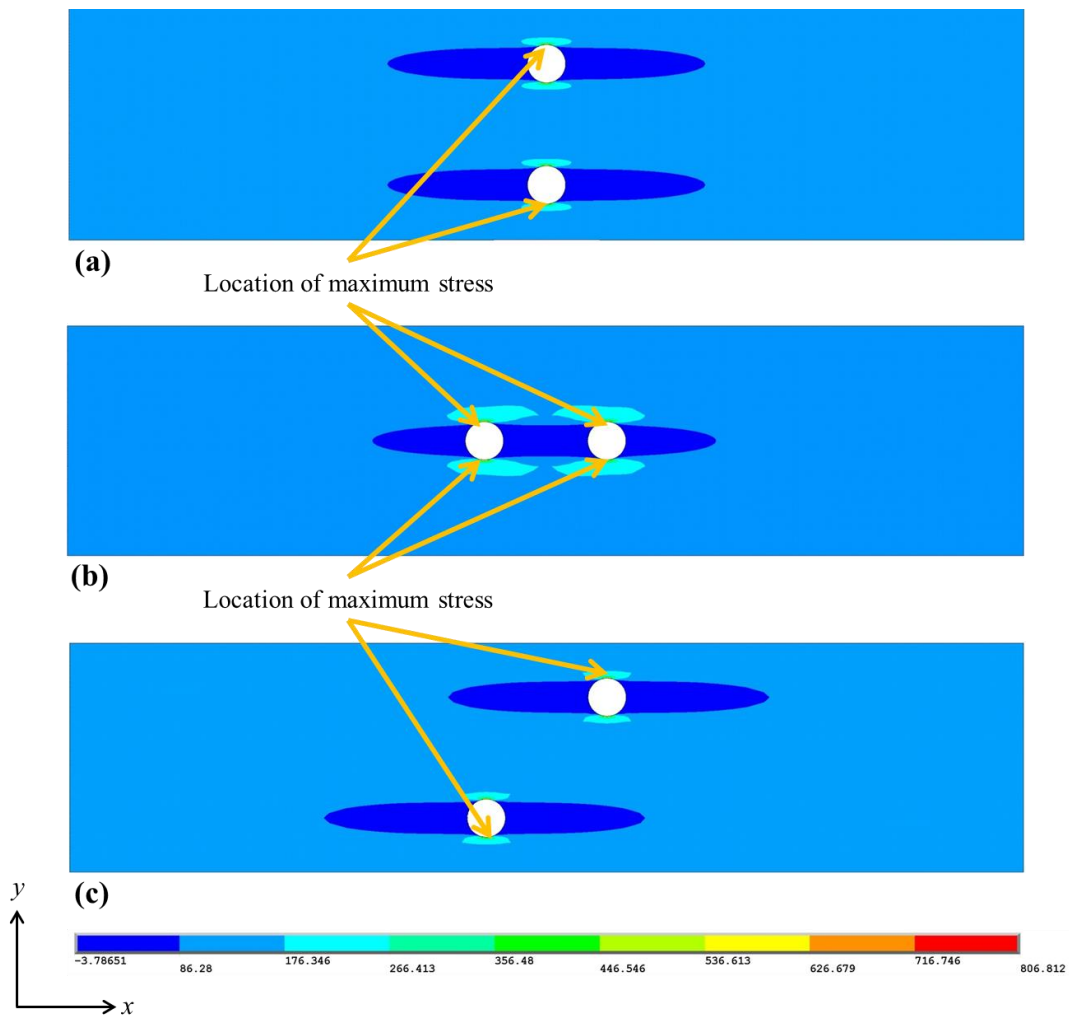
Figure 2.15: σ_{xx} distribution in panel with different hole configurations
(a) 2HL (b) 2HT (c) 2HD

2.6.1 Hashin's failure criterion

Hashin's failure criterion [14] which is a stress based failure criterion is employed for predicting damage initiation as well as damage evolution because of the following reasons. It can predict different modes of failure in a composite structure which is particularly useful for progressive damage modeling because different degradation rules need to be employed for different modes of failure. Hashin's failure criteria is widely used by researchers for strength prediction as well as for progressive failure analysis and good agreement does exist with the experimental prediction [42, 44, 47]. Since it is a 3D failure criterion, Hashin's failure criteria can be employed with 3D FE analysis. Also, it is easy to incorporate in APDL code. Four sets of criteria are set for predicting four different modes of failure. The modes of failure considered in this study are fiber failure under tensile load, fiber failure

43

under compressive load, matrix failure under tensile load and matrix failure under compressive load. The stresses for each element and the material strength values are substituted into Hashin's failure criterion for prediction of damage. Hashin's failure criterion for unidirectional composite laminate is given below [14]:

1. Fiber failure under tensile load

$$\sigma_{xx} \geq 0 \tag{2.1a}$$

$$\left(\frac{\sigma_{xx}}{X_T}\right)^2 + \frac{\sigma_{xy}^2 + \sigma_{xy}}{S_{xz}^2} = \begin{cases} \geq 1 & \text{failure} \\ < 1 & \text{no failure} \end{cases} \tag{2.1b}$$

2. Fiber failure under compressive load

$$\sigma_{xx} < 0 \tag{2.2a}$$

$$\left(\frac{\sigma_{xx}}{X_T}\right)^2 = \begin{cases} \geq 1 & \text{failure} \\ < 1 & \text{no failure} \end{cases} \tag{2.2b}$$

3. Matrix failure under tensile load

$$\sigma_{yy} + \sigma_{zz} > 0 \tag{2.3a}$$

$$\frac{\left(\sigma_{yy} + \sigma_{zz}\right)^2}{Y_T^2} + \frac{\sigma_{yz}^2 - \sigma_{yy}\sigma_{zz}}{S_{xz}^2} + \frac{\sigma_{xy}^2 + \sigma_{xz}^2}{S_{xy}^2} = \begin{cases} \geq 1 & \text{failure} \\ < 1 & \text{no failure} \end{cases} \tag{2.3b}$$

4. Matrix failure under compressive load

$$\sigma_{yy} + \sigma_{zz} < 0 \tag{2.4a}$$

$$\left[\left(\frac{Y_C}{2S_{yz}}\right)^2 - 1\right]\left(\frac{\sigma_{yy} + \sigma_{zz}}{Y_C}\right) +$$

$$\frac{\left(\sigma_{yy} + \sigma_{zz}\right)^2}{4S_{yz}^2} + \frac{\sigma_{yz}^2 - \sigma_{yy}\sigma_{zz}}{S_{yz}^2} + \frac{\sigma_{xy}^2 + \sigma_{xz}^2}{S_{xy}^2} = \begin{cases} \geq 1 & \text{failure} \\ < 1 & \text{no failure} \end{cases} \tag{2.4b}$$

where σ_{ij} denote the stress components. The parameters X_T, Y_T, Z_T denote the allowable tensile strength along the principal material direction whereas X_C, Y_C, Z_C denotes the allowable compressive strength. Further, S_{xy}, S_{xz} and S_{yz} denote allowable shear strength along the respective principal material directions.

2.6.2 Material property degradation method

Once the failure is detected in any of the elements, damage modeling needs to be done for mimicking loss in load carrying capacity of the failed element. One of the damage modeling methods is material property degradation method. The material property degradation can be performed with the finite element method. In this case, damage is assumed to have an effect on the failed elements and the elastic moduli of the failed elements are modified according

to the mode of failure occurred. When failure is detected in an element, dominant elastic material properties are degraded to 5 % of their actual value according to a degradation rule as given in Table 2 [42]. For matrix failure in tension as well as in compression, since the matrix bears load in the y and z directions, Young's modulus values E_{yy}, E_{zz} together with G_{yz} and v_{yz} are degraded. This mode of failure affects only matrix directional properties (properties along transverse directions), therefore other material properties are unaffected. For fiber failure in tension, since fibers are oriented in x direction, Young's modulus value E_{xx} is degraded together with G_{xy}, G_{xz}, v_{xy} and v_{xz}. For fiber failure in compression, E_{xx}, G_{xy}, G_{yz}, G_{xz}, v_{xy} and v_{xz} are degraded. When more than one mode of failure is detected in an element, all the material properties are degraded so that the element cannot take load in any direction. These three steps are repeated up to the complete failure of the panel as shown in the flow chart (see Figure 2.16).

Table 2.2: Material property degradation rules (Fiber orientation is along x direction): (x) property to be degraded, (-) unaffected property

	E_{xx}	E_{yy}	E_{zz}	G_{xy}	G_{yz}	G_{xz}	v_{xy}	v_{yz}	v_{xz}
Tensile matrix mode	-	×	×	-	×	-	-	×	-
Tensile fiber mode	×	-	-	×	-	×	×	-	×
Compressive matrix mode	-	×	×	-	×	-	-	×	-
Compressive fiber mode	×	-	-	×	×	×	×	-	×
More than one failure mode	×	×	×	×	×	×	×	×	×

2.6.3   Implementation

The above mentioned steps of PDM are incorporated in ANSYS parametric development language (APDL) macro-routine and algorithm works in an iterative manner. The implementation of macro-routine is as per the flow chart given in Figure 2.16. A 3D finite element model is initially built by giving as input the initial material properties, dimension of the specimen, boundary conditions, initial displacement and the displacement increment value. Initially, a small initial displacement is given to the model and stresses in each element are estimated. The estimated stresses and the material strength values are substituted into Hashin's failure criterion to check for damage initiation. If none of the elements has failed, then an incremental displacement is applied by a predefined value. If any of the elements has failed, material properties of the failed element are degraded

according to the degradation rule. When material properties are degraded in an element, the load redistributes to other elements, which could then fail at the same load. It is therefore necessary to iterate at the same load level when material properties are degraded to check if other elements undergo failure [42]. After degradation of failed elements, the routine checks for final failure of the laminate. If the final failure has occurred, the routine stops, if not it estimates the redistributed stress values under the same applied displacement. The process is repeated until the final failure has occurred.
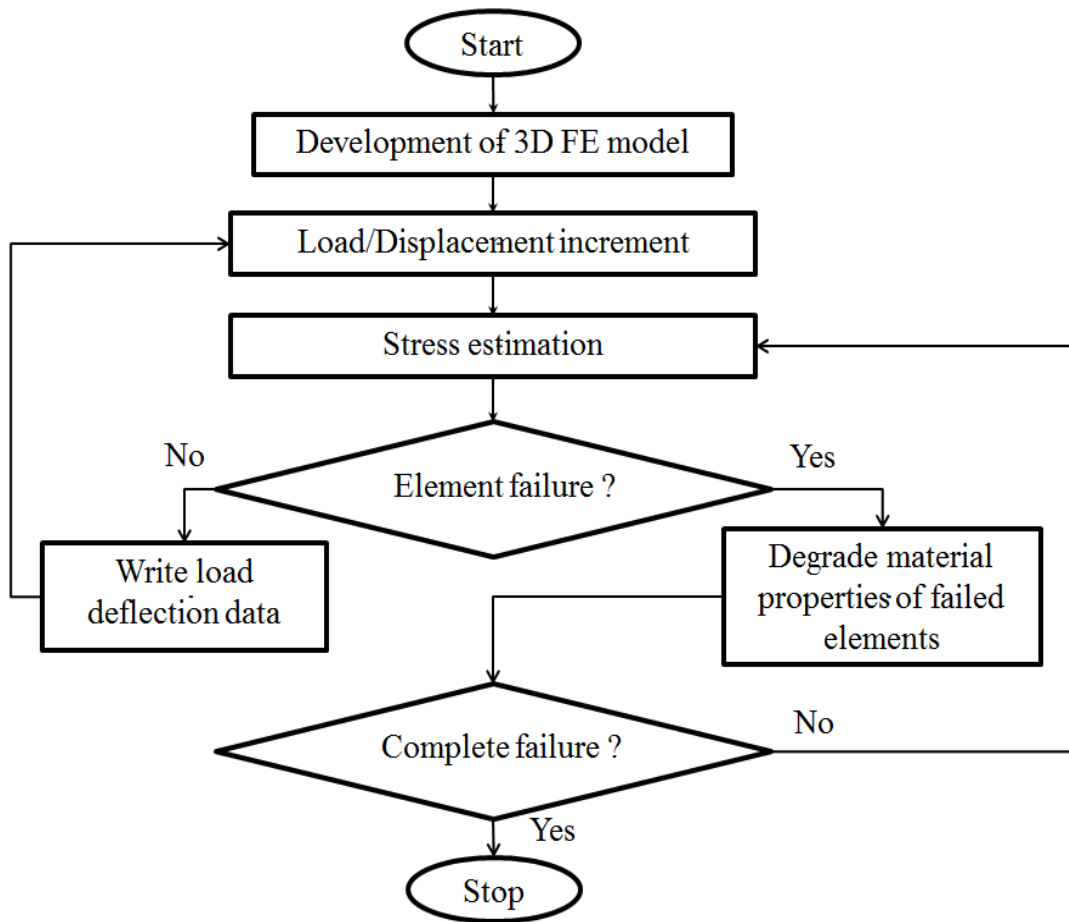
Figure 2.16: Flow diagram of the progressive damage model program

2.7   Results and Discussion

2.7.1   Progressive failure analysis

Load-displacement curves predicted by PDM simulations for composite panels having two holes with different hole configurations are compared with experimental behavior (see Figure 2.17). The behavior from PDM is close to the experimental one. Failure initiation load, at which failure starts (any mode) in any of the element in the panel predicted by

PDM, is given in Table 2.3. Also, ultimate load (load at final failure) from both PDM as well as experiment is given in Table 2.3. It is to be noted that good agreement exists in the load values whereas displacement is under-predicted by FEA. In particular there is a very good match in case of 2HL panel configuration. The choice and implementation of composite failure theory is very critical in the accuracy of PDM prediction. Several composite failure theories perform well in specific cases and poor in others [65], suggesting trial and error basis for selection. Besides this, there are approximations involved in the material property degradation rules as well as in the degradation factors. The above mentioned factors could be the reason for deviation between PDM and DIC results. The various kind of defects occurred during casting of CFRP panels such as presence of air voids, inclusion of foreign bodies, waviness of fiber, misalignment of fiber orientation etc. could affect the experimental results, e.g. misalignment of fibers can result in more displacement of the panel because of the shear deformation in the matrix material.

Longitudinal stress – strain behavior away from the holes is plotted for all the three panel configurations from both PDM and DIC. They are shown in Figure 2.18. Slope of the stress – strain curves obtained from PDM and DIC are found to be in close agreement with the Young's modulus (E_{xx}) value of the composite laminate once again confirming the accuracy of PDM algorithm developed. Load – displacement behavior of composite laminates with different hole configurations are compared using both PDM as well as DIC (see Figure 2.19). It is observed that composite laminate with two holes in longitudinal direction (2HL) sustains highest load before final failure compared to the other two configurations.

Usually there is lot of damage accumulation around the hole due to matrix cracking and the damage always initiate from there and propagate towards the tab end. Figure 2.20 shows the PDM prediction of failure initiation zones near the transverse edge of the holes in panels with different hole configurations. For all the hole configurations studied, matrix failure in tension is predicted by PDM as the first mode of failure initiation and is in line with the literature [6, 66]. Figure 2.21 illustrates the path of damage progression predicted by PDM as well as from experiments for all the panel configurations. It can be clearly seen that PDM predictions match reasonably well with the experimental observations for all the cases thereby confirming the correctness of PDM. In all the hole configurations studied, it is generally observed that damage starts near the transverse edge of holes and propagates in the longitudinal direction due to fiber splitting up to tab end. This kind of failure is very much akin to [0°] fiber laminate.
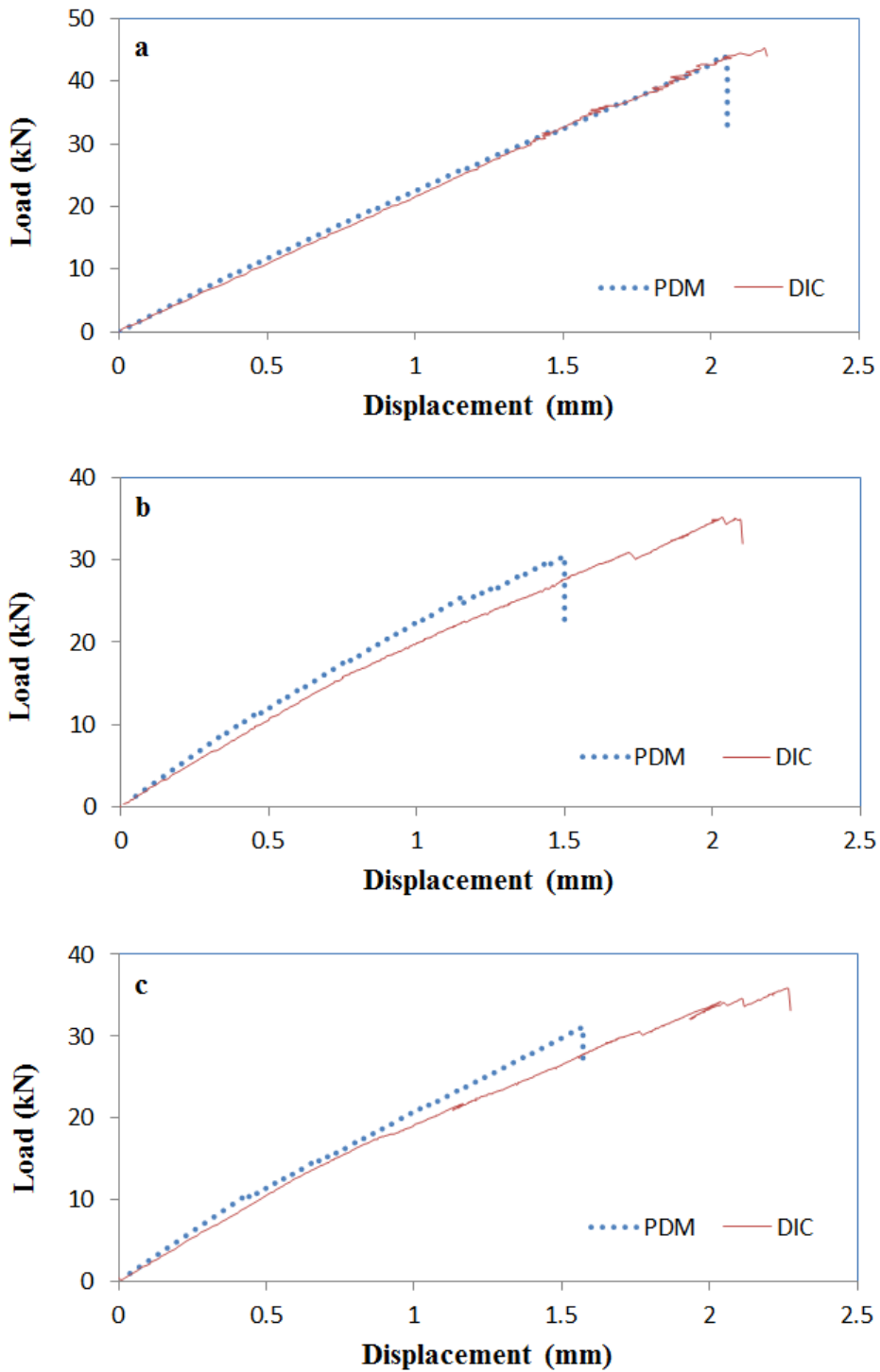
Figure 2.17: Load-displacement behavior for panel with different hole configurations (a) 2HL (b) 2HT (c) 2HD

48
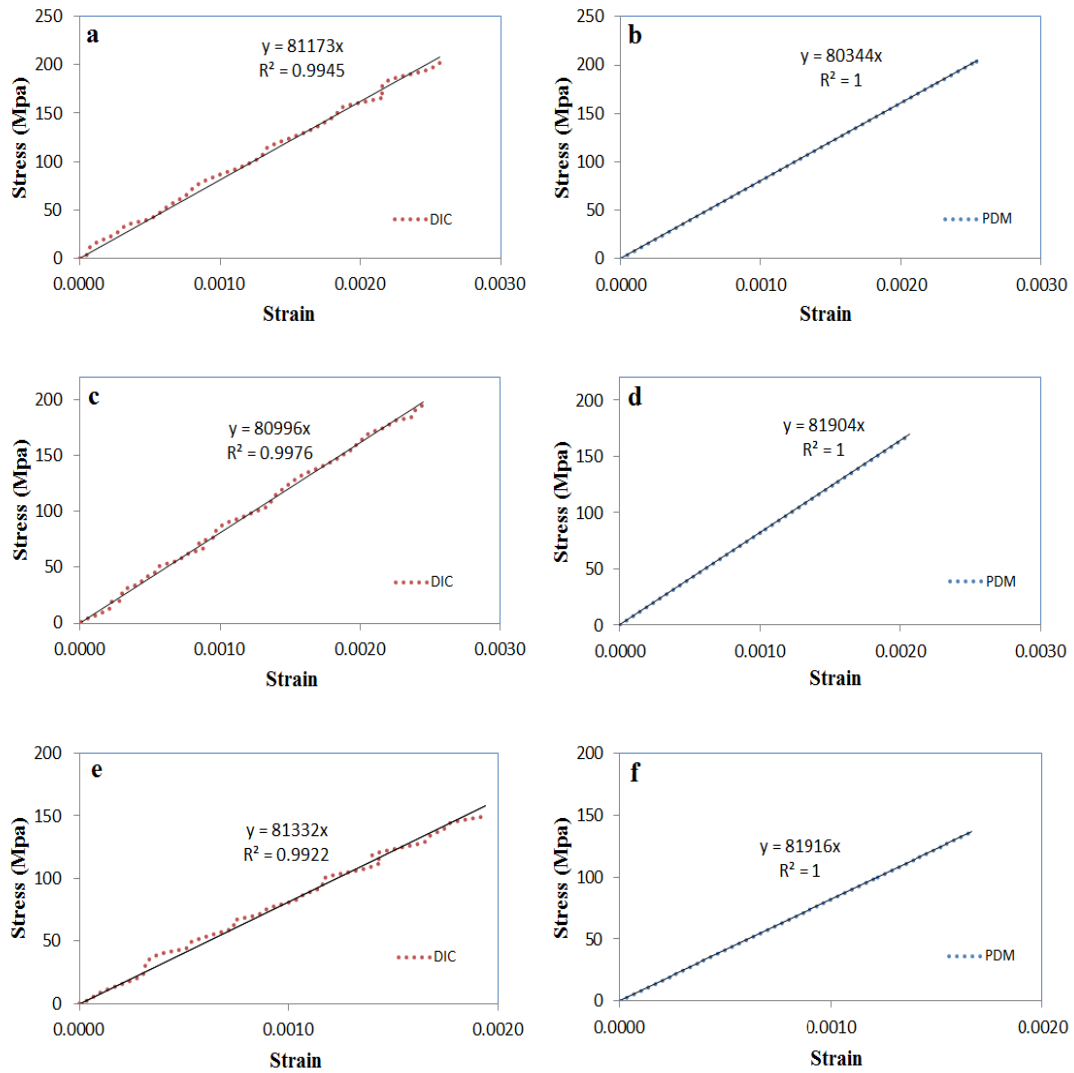
Figure 2.18: Stress-strain curve for different panel configurations far away from hole (a) for 2HL configuration from DIC (b) for 2HL configuration from PDM (c) for 2HT configuration from DIC (d) for 2HT configuration from PDM (e) for 2HD configuration from DIC (f) for 2HD configuration from PDM

Table 2.3: Failure initiation load and ultimate load for panel with different hole configurations

Configuration	Failure initiation load (kN)	Ultimate load (kN)	
	PDM	Experiment	PDM
2HL	4.868	45.267	43.695
2HT	3.394	35.20	30.506
2HD	3.69	35.801	31.089
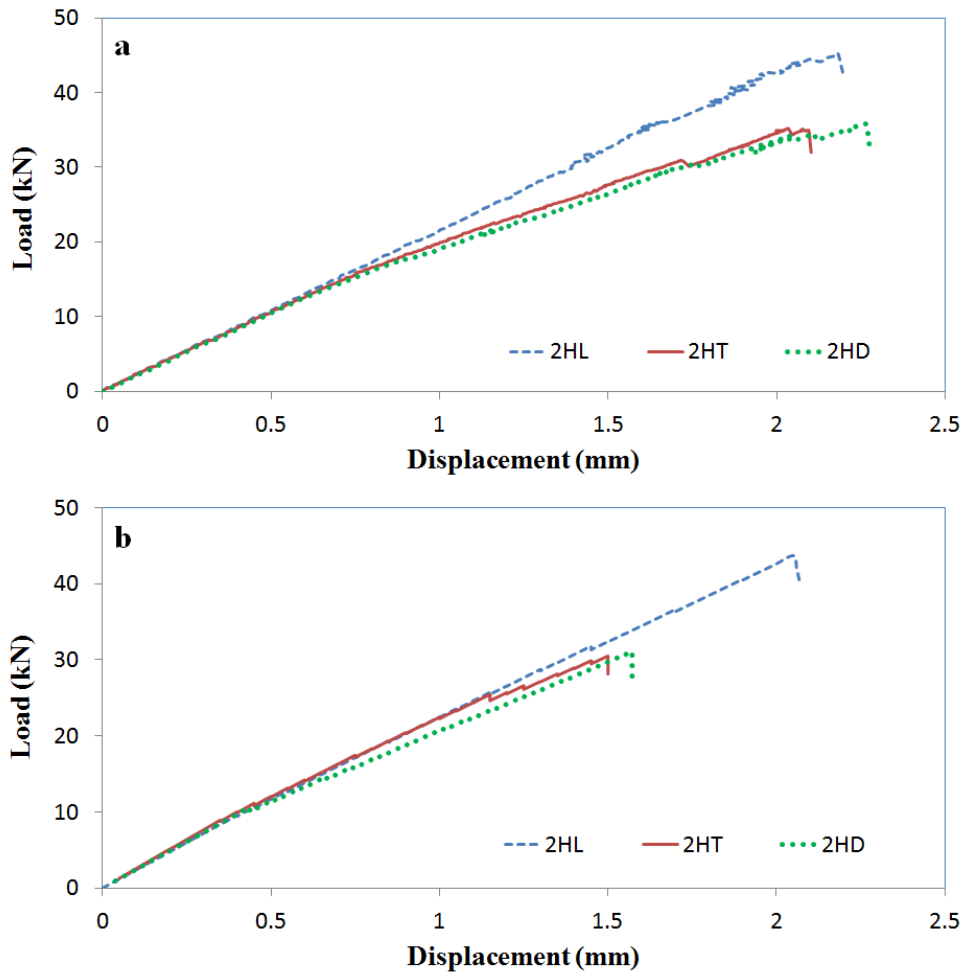
Figure 2.19: Load-displacement behavior for panel with different hole configurations (a) DIC (b) PDM

2.7.2 Effect of hole spacing on stress concentration factor

Figure 2.22 illustrates the effect of hole spacing on SCF for panel with different hole configurations. It can be seen that for 2HL configuration, SCF decreases as hole spacing (SL) decreases as shown in Figure 2.22a. It is because as the hole spacing increases, the ineffective region of the laminate which do not carry any load increases and the stress flux redistributes within this zone. There is a shielding effect and the stress flux lines are diverted away from the hole if they are closer. Therefore a closer spacing of holes is preferred in this configuration. For 2HT configuration, stress interaction between two holes becomes more severe when holes are placed closer to each other (see Figure 2.22b). As hole spacing (ST) is being increased from 1.5D to 2.5D (where D is the diameter of hole), SCF keeps on reducing. But for hole spacing greater than 2.5D, it is observed that SCF increases

as hole spacing increases because of increasing stress interaction between hole edge and free edge. Optimum spacing where SCF becomes least is found to be 2.5*D* in this case. In case

2HL

(a)   (b)

2HT

(a)   (b)

2HD

y

(a)   ▉ Matrix failure   (b)

x
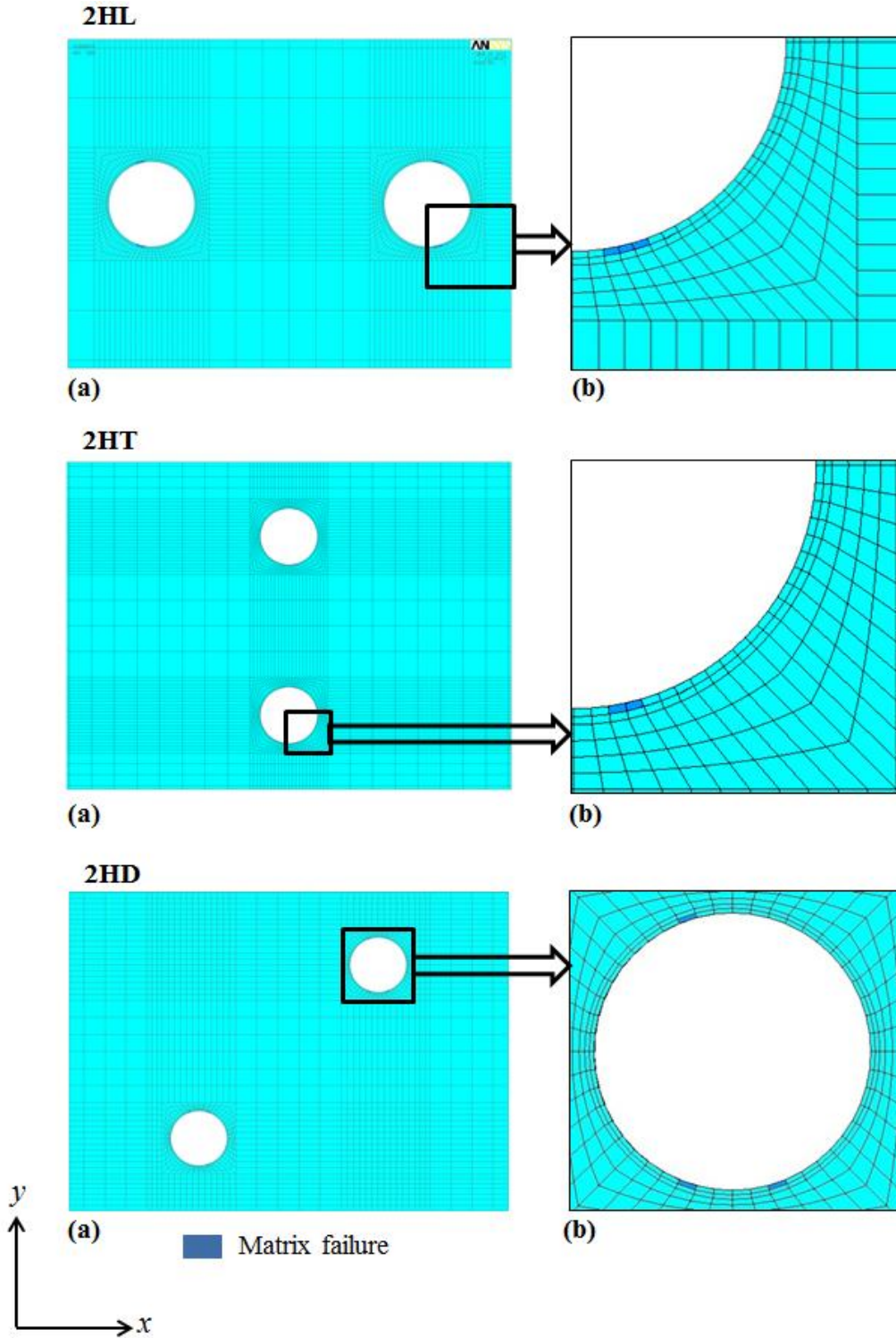
Figure 2.20: Failure initiation location for panel with different hole configurations (a) overall view (b) zoomed up view showing failure initiation

of panel having 2HD configuration, for spacing variation in transverse direction (ST) from 1.5D to 2.5D, SCF decreases with increase of spacing in longitudinal direction (SL) as shown in Figure 2.22c. It is because of the lesser stress interaction between two holes as longitudinal spacing increases. But in case of transverse spacing greater than 2.5D, SCF increases as longitudinal spacing increases because of hole edge to specimen edge stress interaction effects. In this case, transverse spacing of 2D to 3D is preferable. Transverse spacing of 1.5D and 4D are not recommended as it results in higher SCF values.
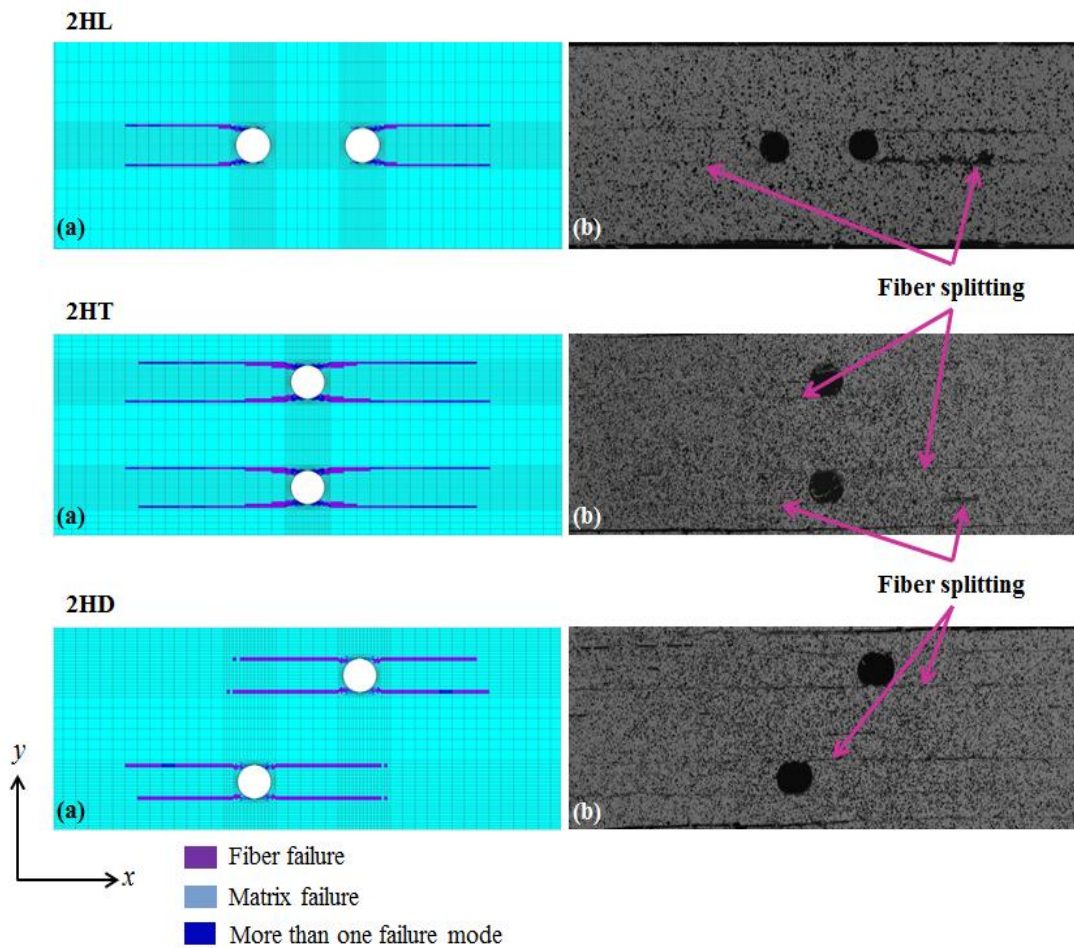
Figure 2.21: Damage propagation in panel with different hole configurations (a) PDM prediction (b) experiment
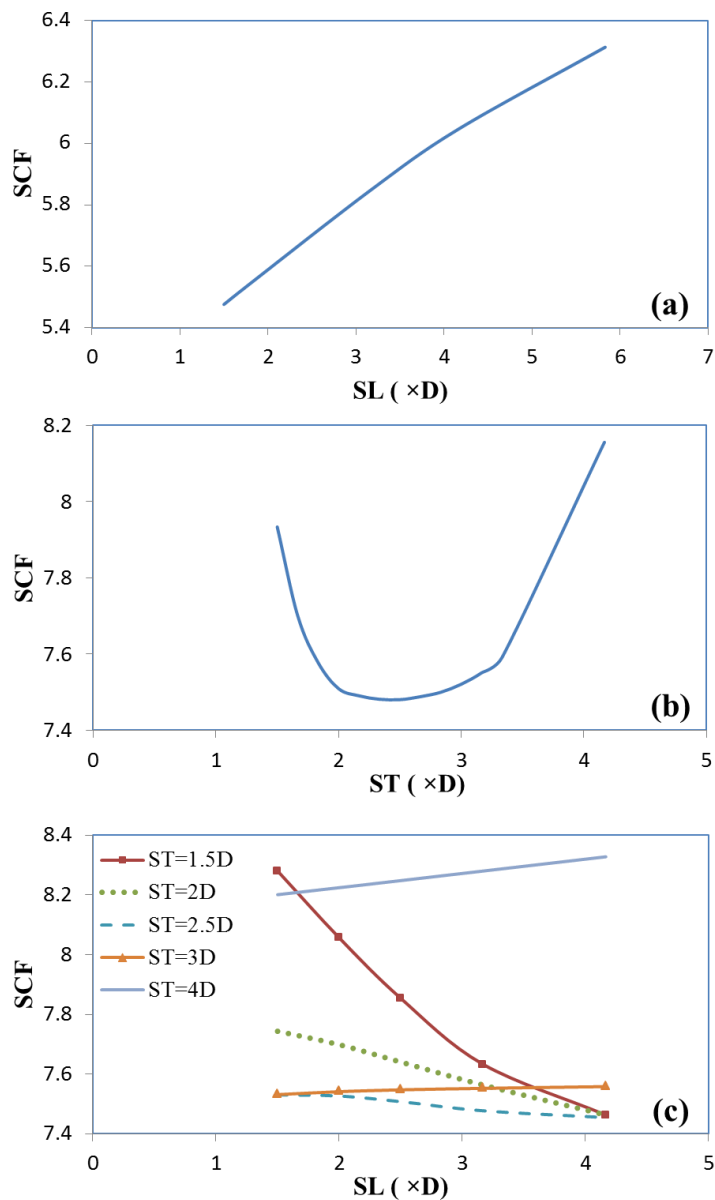
Figure 2.22: Effect of hole spacing on SCF in panel having different hole configurations (a) 2HL (b) 2HT (c) 2HD

2.8   Closure

A 3D finite element based PDM is developed for composite laminates having two holes of different configurations subjected to in plane tensile load. Hashin's failure criteria is used for damage prediction and material property degradation method is implemented for damage evolution. Finite element model is first validated by comparing whole field surface strains and displacements obtained from FEA with those from DIC experiment. They are found to be in good agreement. The PDM algorithm developed is able to predict different modes of failure, load – deflection behavior and damage progression up to final failure for different

panel configurations. Load – deflection behavior predicted by PDM is also compared with the experimental behavior and is found to be in good agreement. Among different hole configurations studied, the 2HL laminate has sustained maximum load of 45.267 kN which is 28.7 % and 26.4 % more than 2HT and 2HD configurations respectively. For all the hole configurations, damage initiates as matrix failure under tension at transverse edge of the holes and progresses in the longitudinal direction towards tab end causing fiber splitting. Path of damage progression predicted by PDM is also in coherence with the experimental observations there by confirming the accuracy of the PDM algorithm developed. Effect of hole spacing on SCF for panel with different hole configurations is further investigated. For 2HL configuration, SCF decreases as hole spacing decreases whereas for 2HT configuration, stress interaction becomes more severe when holes are placed closer to each other. Therefore, closer spacing of holes are needed in 2HL configuration whereas closer spacing of holes has to be avoided in 2HT configuration. In case of 2HT configuration, more spacing can lead to higher stress interaction between hole edge and free edge. For panel with 2HD configuration, when holes are placed closely in the transverse direction, SCF decreases with increase in longitudinal spacing. As spacing in transverse direction increases, SCF also increases with longitudinal spacing.

Chapter 3

Progressive Damage Model for Multi-Pin Joints in Composite Laminates

3.1   Introduction

In this chapter, a 3D finite element based PDM is presented for double- lap, multi-pin joints in unidirectional CFRP laminates subjected to tensile loading. The developed model is suitable for predicting failure and post failure behavior of pin joints in fiber reinforced composite materials. It can also predict the final failure modes near the pin loaded holes. The material is assumed to behave as linear elastic until final failure. The stress values are estimated using 3D finite element analysis and damage prediction is done using Hashin's failure criterion for unidirectional composite laminates as explained in previous chapter. Damage modeling is accomplished using MPDM [42-43, 45]. DIC experiment is carried out to perform whole field strain analysis of CFRP panels. Whole field surface strain and displacement from finite element prediction are compared with DIC results for validation of the finite element model. Load-deflection behavior as well as path of damage progression is predicted by both PDM simulation and experiment. They are found to be in good agreement thereby confirming the accuracy of PDM implementation. The modes of final failure near the pin loaded holes are predicted by PDM which are in coherence with the experimental observation.

The longitudinal as well as transverse spacing between pin loaded holes affect greatly on the behavior of the pin joint. The maximum longitudinal stress value in a panel with multiple holes changes as the spacing between holes changes. Therefore the damage behavior is also influenced by the spacing between holes. The effect of spacing between the holes on the stress levels in the panels is further investigated in this chapter involving FEA.
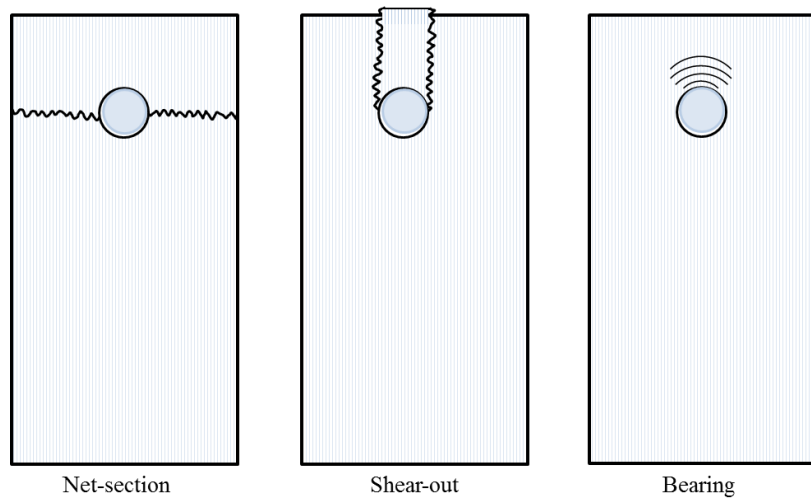
Figure 3.1: Illustration of three basic failure modes

According to experimental evidence, pin joints under tensile loads generally fail in three basic modes referred to as net-section, shear-out and bearing [5]. The net-section mode is abrupt, with a well-defined failure load, whereas bearing and shear-out usually are more ductile [5, 51]. Different type of damage resulting from each of these modes is shown in Figure 3.1.
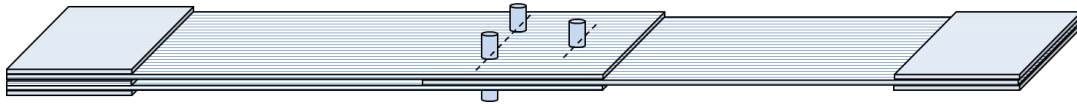
Figure 3.2: Double-lap, Multi-pin joint studied
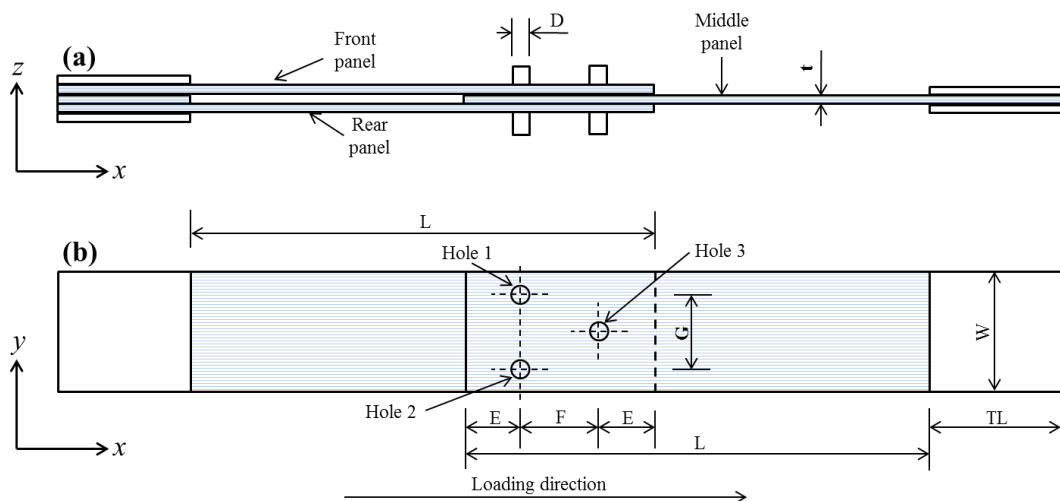
Figure 3.3: Geometry of the double-lap, three-pin joint specimen
(a) Front view (b) Top view

3.2   Problem Description

In the present study, double-lap, three-pin joints of unidirectional Carbon/Epoxy composite laminate is considered as shown in Figure 3.2. Panel is having a layup of $[0^o]_8$ configuration. The geometry of double-lap, three-pin joint is shown in Figure 3.3. The length (L), width (W) and the thickness (t) of the panel are 182 mm, 44 mm and 3.1 mm respectively. Diameter (D) of the hole is 6 mm. Tab length (TL) is taken as 50 mm. First and second pins are symmetric with respect to the center line of the specimen by a distance of 24 mm (G) and are located a distance 18 mm (E) from the free edge of the specimen. The third hole is located along the center line of the plate at a horizontal distance 24 mm (F) from the first and second pins. Mild steel pins of 6 mm diameter (D) and 15 mm length (H) are used. Left end of the front and rear panels are fixed and an in-plane incremental tensile load is applied to the right end of the middle panel. The fibers are aligned along the loading direction.

3.3   Experimental Analysis involving DIC

In this study, double-lap, three-pin joints in CFRP laminates is considered. Geometry of the specimen is already described in section 3.2. As mentioned in section 3.2, three panels of unidirectional CFRP are joined using three steel pins. Experiment results are used for the validation of finite element model and also of the progressive damage model.

3.3.1   Specimen preparation

Composite panels are prepared as per the dimensions described in section 2.3.1. Unidirectional carbon fiber mat of 220 gsm is used. Aluminium tabs of required dimension are bonded to the test specimen using AV138/HV998 adhesives. Tabs are provided at the end of the specimen for obtaining a better grip and to avoid damage while specimen is loaded in the MTS machine. Also, a CFRP sheet of required dimension is placed between the two panels in the griping end to ensure in-plane loading condition. Mild steel pins of required dimensions are made by turning and facing operation in the lathe machine. Prepared specimen is shown in Figure 3.4. Two radial holes are drilled at the end of each pin and Cotter pins are inserted through these holes for holding them in position. Random speckle patterns are created over the specimen surface using acrylic paints of black and white color to perform DIC experiments. Finally speckle pattern are created over specimen surface as described in section 2.3.1. Figure 3.5 show the specimen applied with speckle pattern.
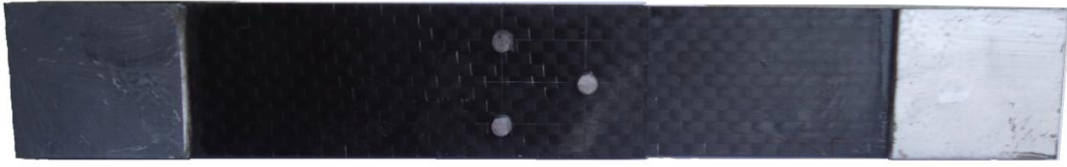
Figure 3.4: Double-lap, three-pin joint in CFRP laminates
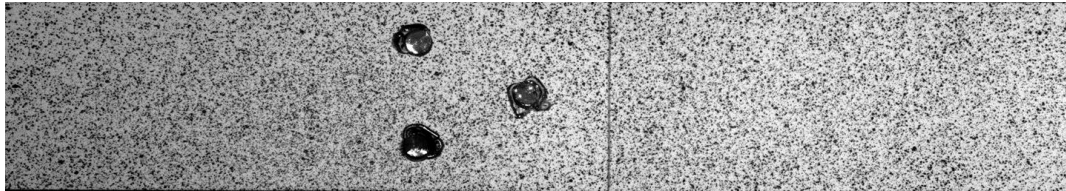
Figure 3.5: Specimen surface applied with speckle pattern

3.3.2 Experimental test procedure

The experimental setup used for present study is shown in Figure 3.6. Experiments are carried out at room temperature using an MTS Landmark® servo-hydraulic cyclic test machine of 100 kN capacity together with a 3D-DIC system (supplied by Correlated Solutions, Inc.) is used which consists of two 8-bit Grasshopper® CCD Cameras (POINTGREY - GRAS-50S5M-C) with a resolution of 2448 x 2048 pixels, coupled with Schneider Xenoplan lenses of 17 mm focal length. The experimental arrangement is explained in section 2.3.2. Figure 3.7 shows the close view of the specimen fixed in hydraulic wedge grips. Vic-Snap 2009 software is used for image grabbing and calibration. Images are grabbed at predefined interval of time while applying uniaxial tensile load at a cross head speed of 1 mm/minute. Load and displacement values are stored corresponding to every image being grabbed using a data acquisition card which interfaces image grabbing system with the MTS controller system. The test is aborted when the final failure has occured. Figure 3.8 shows the final failure of the middle panel. Full field in-plane displacement fields need to be estimated from the captured images. In this study, VIC-3D 2010 software from Correlated Solutions is used for estimating displacement and strain fields.

3.3.3 Material characterization of carbon/epoxy composite laminates

Material properties of the carbon/epoxy composite laminates are determined at room temperature using DIC as given in Ref. [60-61] and they are as per ASTM standards. Procedure followed for determining the material properties for Carbon/Epoxy Composite

Laminates is explained in section 2.3.3. The material properties of Carbon/Epoxy composite laminate obtained from the experiments are given in Table 3.1.
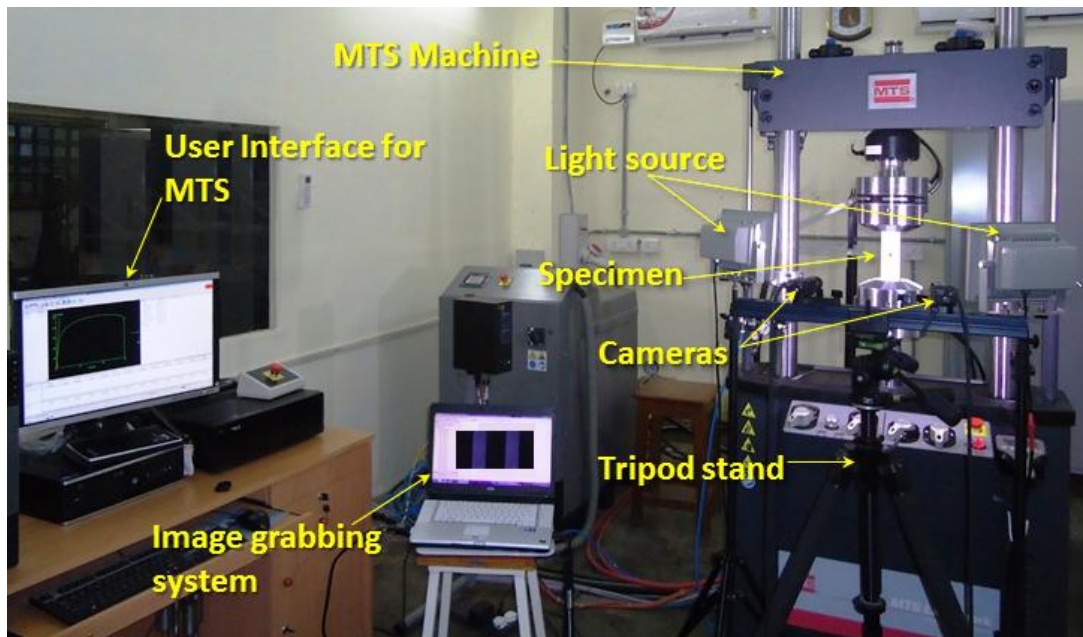
Figure 3.6: Experimental setup
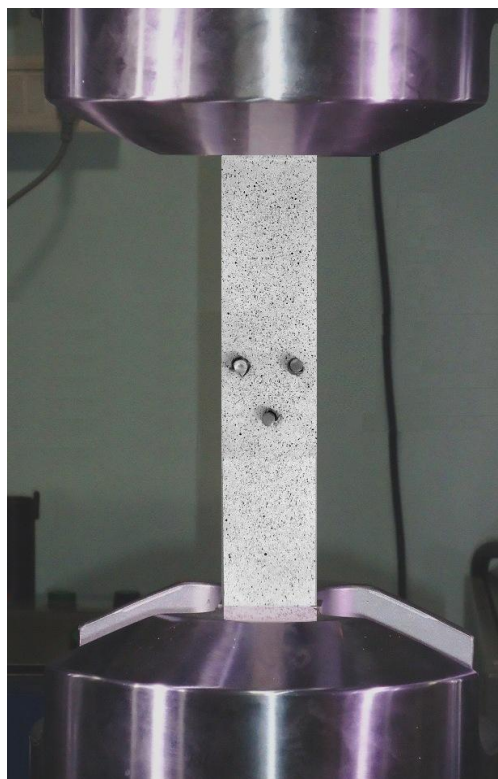
Figure 3.7: Specimen fixed in hydraulic wedge grips

Figure 3.8: Image showing final failure of the middle panel

Table 3.1: Material properties of the carbon/epoxy laminate

Material properties	
Longitudinal modulus , E_{xx} (GPa)	84.6
Transverse modulus, $E_{yy} = E_{zz}$ (GPa)	7.12
Shear moduli, $G_{xy} = G_{xz}$ (GPa)	3.30
Shear modulus, G_{yz} (GPa)	2.47
Poisson's ratio (v_{xy})	0.31
Poisson's ratio (v_{xz})	0.31
Poisson's ratio (v_{yz})	0.43
Longitudinal tensile strength, X_T (MPa)	1080
Transverse tensile strength, Y_T (MPa)	35
Longitudinal compressive strength, X_C (MPa)	600
Transverse compressive strength, Y_C (MPa)	90
Shear strength, $S_{xy} = S_{xz}$ (MPa)	57
Shear strength, S_{yz} (MPa)	28.5

3.4   Finite Element Model

This section focuses on the development of 3D finite element model of the multi-pin joint. A typical FE mesh is shown in Figure 3.9. It is done using ANSYS 13 which is a commercially available finite element package. The panel and pin are modeled using SOLID 186 element, which is a 20 noded brick element. Initially, two dimensional areas are made as per the model dimensions and is meshed with mesh 200 element having 8 nodes. Later, all the areas are extruded in thickness direction to generate volumes. The area mesh is the swept in the thickness direction throughout the volume for solid element meshing. The mesh sweeping is done using SOLID 186 element. The mesh pattern surrounding the hole is

kept very fine in order to capture the high stress gradient around it. The mesh around the circular hole has a total of 9216 elements (96 circumferential; 12 Radial; 8 elements through the thickness). The number of elements along circumferential direction is chosen based on the mesh convergence study as explained in chapter 2. Material properties obtained from DIC based characterization tests are applied to the finite element model. For all the cases, full models are analyzed since symmetry is lost after the damage development. The contact between the overlapping surfaces of panels as well as between surface of the holes and pins are simulated using surface to surface CONTA174 elements together with TARGE170 elements. The contact algorithm employed is augmented Lagrange method. Study is carried out with considering friction and without considering friction. During the analysis, ANSYS checks each contact status to determine if it is in-contact, near-contact, or not near contact. A circular or spherical region called pinball region around each contact (or target) element is used to confirm it. Convergence failure can occur when no contact is detected between contact surfaces. Sometimes the contact elements do not engage because the faces are too far apart, i.e., outside of the pinball. This can also happen when too much penetration occurs and the contact element passes beyond the pinball zone. A larger pinball region could prevent this problem but it increases the computational cost since time taken in searching for contact depends on the size of the pinball region. To avoid the difficulty in obtaining convergence at higher loads and also when more number of elements are degraded, radius of the pinball region is chosen to be 2.6 mm by trial and error method. Normal and tangential stiffness values also could affect the convergence and accuracy of the solution [52]. It is found that default values of normal and tangential stiffness gives quick convergence, small interpenetration and satisfactory accuracy of the strain values in this study. Also, a gradual loading with a maximum of 60 subsets is given to ensure solution convergence.

3.4.1 Boundary conditions

The degree of freedom along x-direction is constrained on left end faces of the front and rear panels. In addition, on left end faces of the front and rear panels, nodes along $z = 0$ are constrained in z-direction and nodes along $y = 0$ are constrained in y-direction. The degree of freedom along x-direction of all the nodes on right end faces of the middle panel is coupled together and displacement in x-direction (u) is applied at the master node which is located at the center of that face.
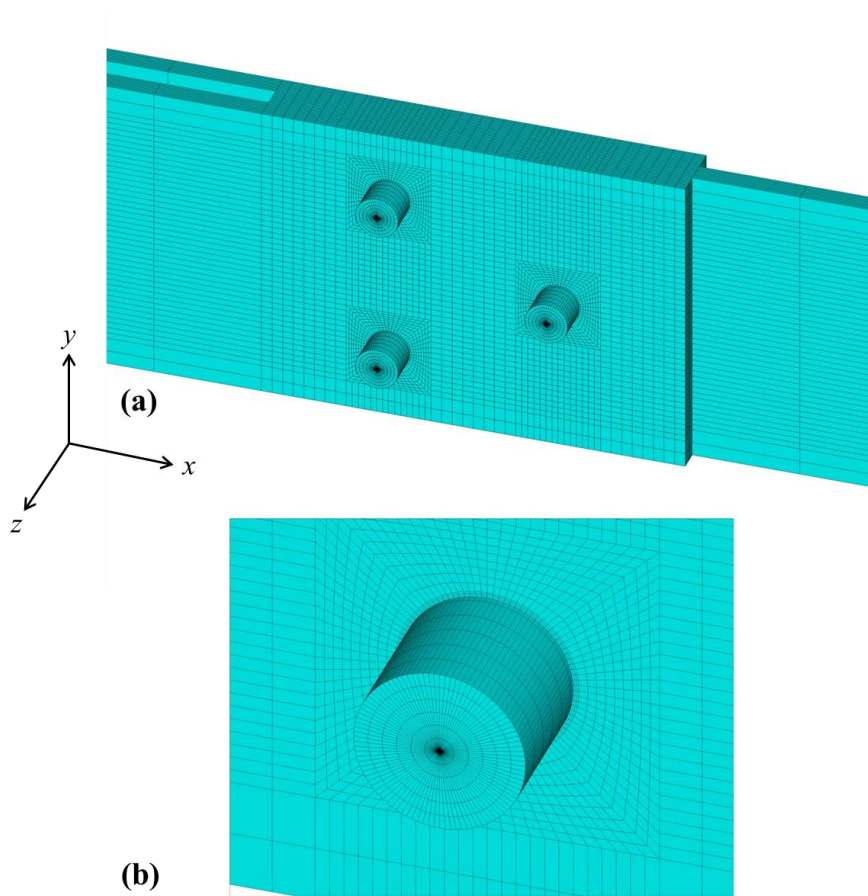
Figure 3.9:Finite element model of multi-pin joint laminate (a) portion of laminate (b) zoomed view around the pin

3.5   Finite Element Model Validation

Initially whole field surface displacement and strain from FEA are compared with those from DIC experiment for validating the finite element model. This is done to make sure that the load, boundary conditions and mesh requirement pertaining to the finite element model are accurate or adequate enough to replicate the experimental behavior of the double-lap three-pin joint laminate. Also the material property definition and input can be verified. Whole field displacement field from both DIC and FEA is compared with each other (see Figure 3.10). One can observe that a good agreement exists between FEA and DIC displacement values. Figure 3.11 shows the whole field ε_{xx} strain distribution on the front panel obtained from both DIC and FEA. Variation of ε_{xx} strain along a line from one free edge to other free edge (see Figure 3.11) at a load of 3.54 kN is given in Figure 3.12. Similarly, whole field ε_{xy} strain distribution is given in Figure 3.13 and variation of ε_{xy} strain along a line from one free edge to other free edge is shown in Figure 3.14. It can be observed that a close quantitative agreement exists between FEA and DIC strain values

thereby confirming the accuracy of finite element model. A polar coordinate system is defined in the center of third hole of the middle panel as illustrated in Figure 3.15. σ_{rr}, $\sigma_{\theta\theta}$ and $\tau_{r\theta}$ variation inside the third hole in the middle panel with friction ($\mu = 0.3$) and without friction ($\mu = 0$) are plotted in Figure 3.16. It can be seen that compressive radial stresses are maximum at the contact center ($\theta = 0^{\circ}$). When friction is considered, there is a reduction in the compressive radial stresses. This is because of the load transfer taking place due to friction in the contact region. Maximum values of circumferential stresses ($\sigma_{\theta\theta}$) is found to be in the hole edges ($\theta = 90^{\circ}$). Also, introduction of friction causes small variation in the circumferential stress values. The shear stress ($\tau_{r\theta}$) is greatly affected by friction. It is because the friction induced shear stresses are proportional to the coefficient of friction [67]. So, higher values of coefficient of friction causes higher shear tractions on the contact surfaces.
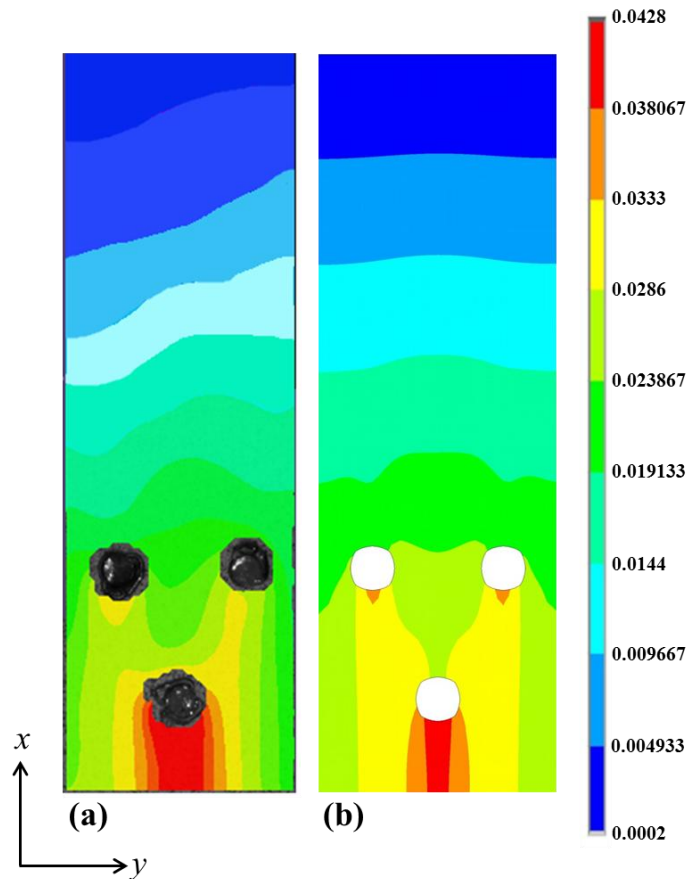
Figure 3.10: Whole field surface *u*-displacement in the front panel at 3.54 kN

63
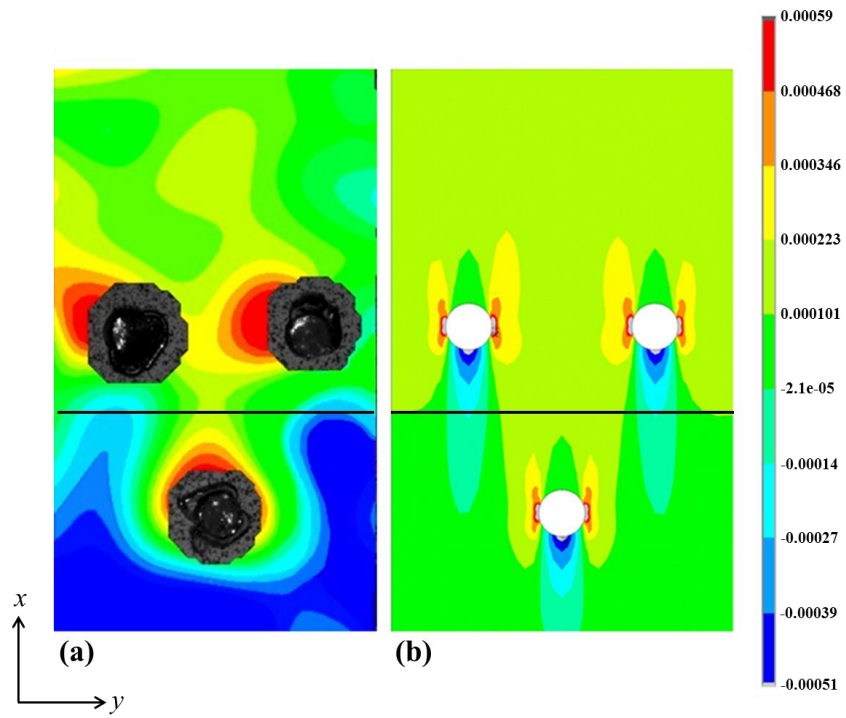
Figure 3.11: Whole field ε_{xx} surface strain distribution in the front panel of composite joint at 3.54 kN load (a) DIC (b) FEA
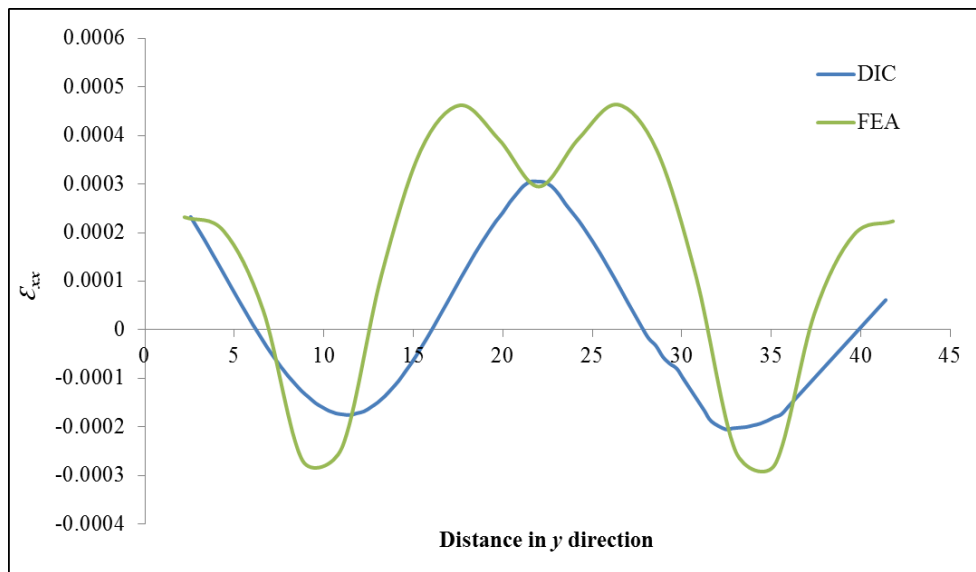
Figure 3.12: ε_{xx} strain variation from one free edge to other free edge of the front panel at 3.54 kN load

64
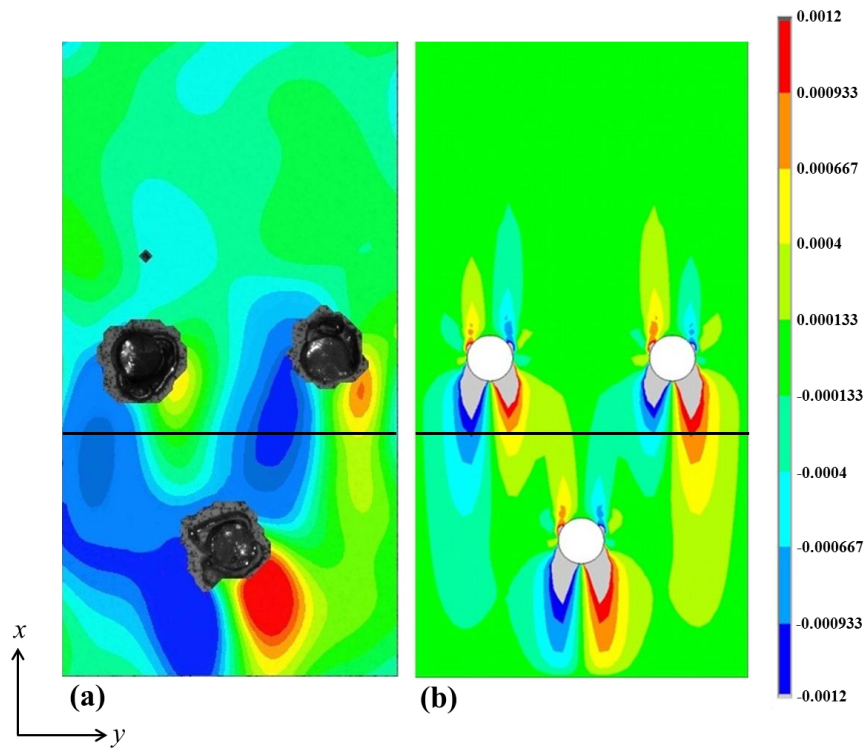
Figure 3.13: ε_{xy} **strain variation from one free edge to other free edge of the front panel at 3.54 kN load**
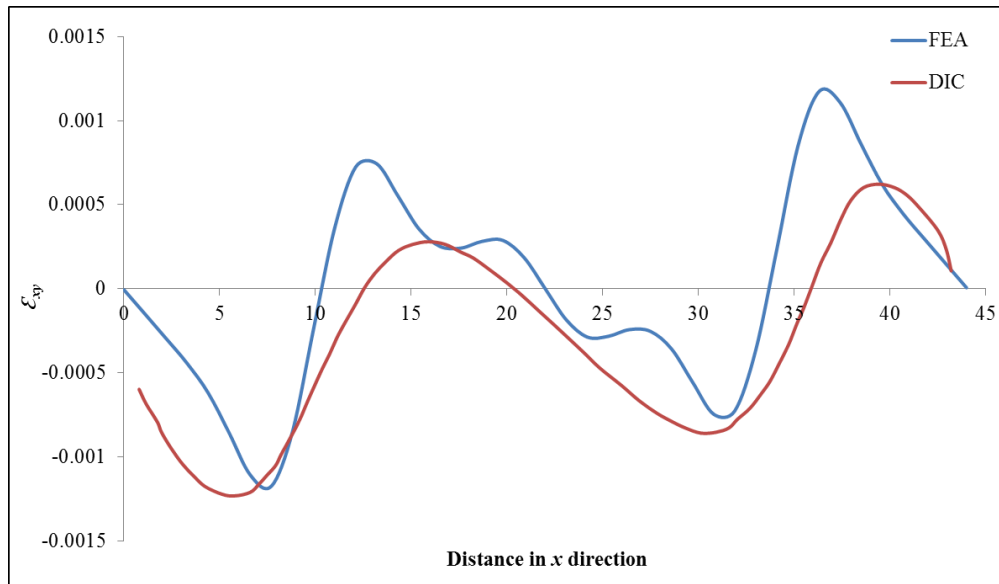
Figure 3.14: ε_{xy} **strain variation from one free edge to other free edge of the front panel at 3.54 kN load**
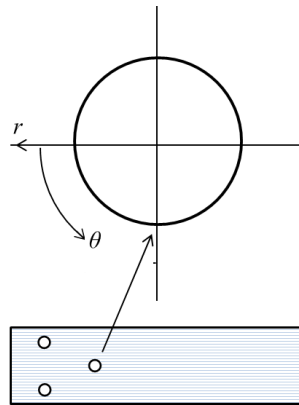
Figure 3.15: Polar coordinate system defined in the center of third hole in the middle panel
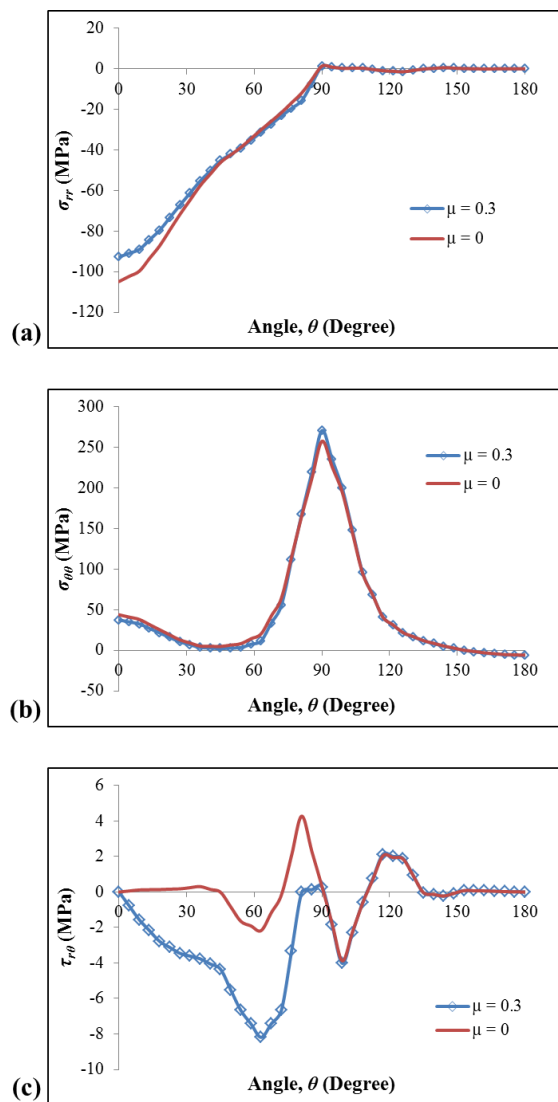
Figure 3.16: Stress variations inside the third hole of the middle panel with friction and without friction (a) σ_{rr} (b) $\sigma_{\theta\theta}$ (c) $\tau_{r\theta}$

3.6   Progressive Damage Model

Progressive damage modeling is performed as explained in section 2.6 by considering different values of coefficient of friction. Stress analysis is done by FEM involving ANSYS 13 commercial finite element package. In this step, stresses are estimated for each element in the principal material direction of the laminate. Figure 3.17 shows the σ_{xx} stress distribution and the location of maximum stress in the middle panel. Hashin's failure criterion [14] is used and it is a stress based failure criterion generally employed for damage prediction. In this work, same Hashin's failure criterion is employed here and exactly the same PDM model is implemented as explained in Chapter 2.
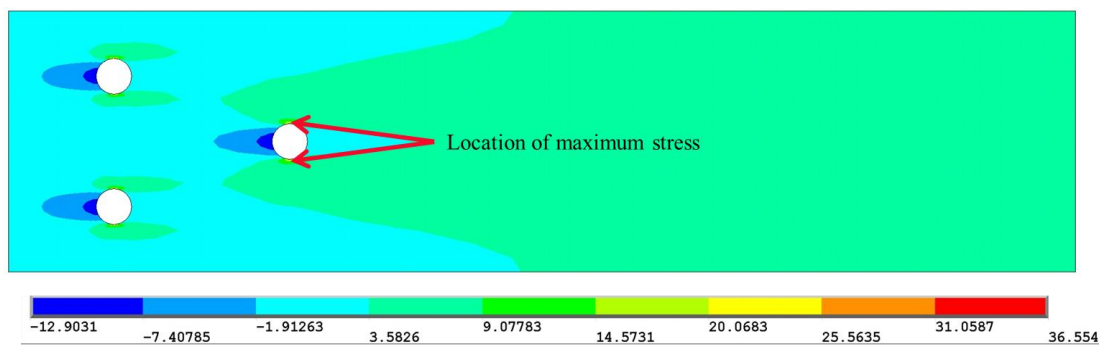
Figure 3.17: σ_{xx} **distribution in the middle panel**

3.6.1   Material property degradation method

In this study damage modeling is achieved by material property degradation methods as discussed in section 2.6.2. When failure is detected in an element, dominant elastic material properties are degraded to 5 % of their actual value according to a degradation rule as given in Table 3.2. Degradation rules for tensile and compressive failure of fiber and matrix are taken from Ref. [42] and degradation rules for fiber-matrix shear and delamination failures are taken from Ref. [52]. For matrix failure in tension as well as in compression, since the matrix bears load in the y and z directions, Young's modulus values E_{yy}, E_{zz} together with G_{yz} and v_{yz} are degraded. This mode of failure affects only matrix directional properties (properties along transverse directions), therefore other material properties are unaffected. For fiber failure in tension, since fibers are oriented in x direction, Young's modulus value E_{xx} is degraded together with G_{xy}, G_{xz}, v_{xy} and v_{xz}. For fiber failure in compression, E_{xx}, G_{xy}, G_{yz}, G_{xz}, v_{xy} and v_{xz} are degraded. When more than one mode of failure is detected in an element, all the material properties are degraded so that the element cannot take load in any direction. These three steps are repeated up to the complete failure of the panel as shown in the flow chart (see Figure 2.16).

67

3.6.2   Implementation

The above mentioned steps of PDM are incorporated in ANSYS parametric development language (APDL) macro-routine and algorithm works in an iterative manner. The implementation of macro-routine is as per the flow chart given in Figure 2.16 and is explained in detail in section 2.6.3.

3.7   Results and Discussion

3.7.1   Progressive failure analysis

Load-displacement curves are predicted by PDM for double-lap, three-pin joint in composite panels by considering different values of coefficient of friction (μ). They are compared with experimental behavior (see Figure 3.18). It can be observed that as coefficient of friction increases, the load carrying capacity increases. It is because of more load transfer that happens due to frictional forces in case of model with higher coefficient of friction. The behavior from PDM with $\mu = 0.25$ is found to be close to the experimental one. Failure initiation load, at which failure starts (any mode) in any of the element in the panel predicted by PDM, is given in Table 3.3. Also, final failure load from both PDM as well as experiment is given in Table 3.3. Maximum load carried by the composite joint is taken as the final failure load [52]. The models with lower coefficient of friction predict lower failure initiation load and final failure load. It is because, when friction is more, load is transferred through larger area due to frictional forces, reducing the stress concentration. It is to be noted that good agreement with experimental value exists in the final failure load value for $\mu = 0.25$. The choice and implementation of composite failure theory is very critical in the accuracy of PDM prediction. Several composite failure theories perform well in specific cases and poor in others [65], suggesting trial and error basis for selection. Besides this, there are approximations involved in the material property degradation rules as well as degradation factor value. The above mentioned factors could be one of the reasons for deviation between PDM and DIC results.

Table 3.3: Failure initiation load and final failure load for panel with different hole configurations

Failure initiation load (kN)					Final failure load (kN)				
PDM				Experiment		PDM			
$\mu = 0$	$\mu = 0.15$	$\mu = 0.25$	$\mu = 0.3$			$\mu = 0$	$\mu = 0.15$	$\mu = 0.25$	$\mu = 0.3$
4.92	5.04	5.232	5.513	14.17		12.02	13.05	13.90	16.03
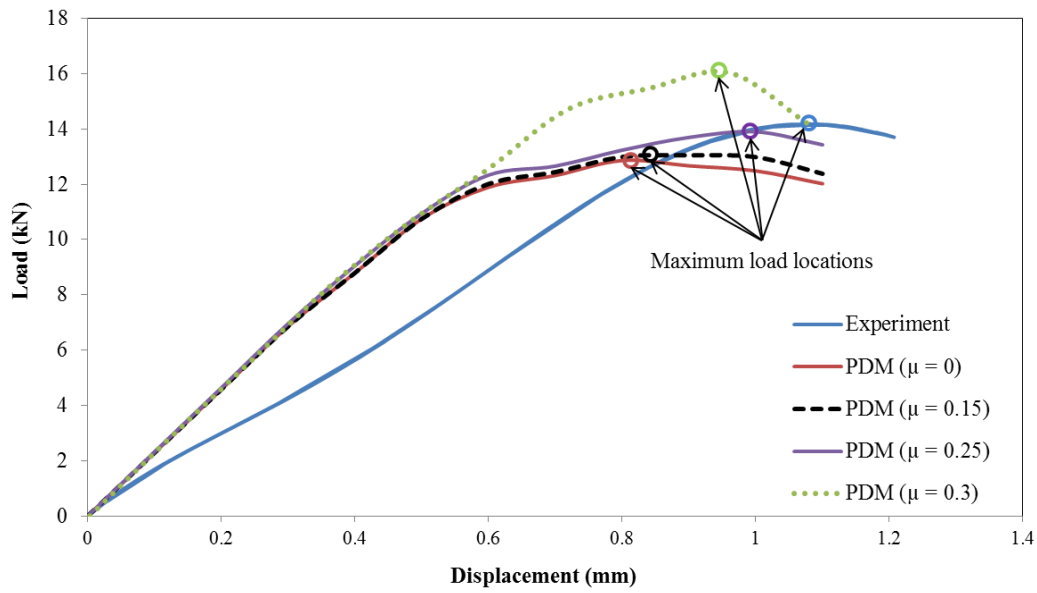
Figure 3.18: Load-displacement behavior of the composite joint

Figure 3.19 shows the PDM prediction of failure initiation zones near the longitudinal edge of the third hole. Matrix failure in tension is predicted by PDM as the first mode of failure initiation nearer to all the three holes. Figure 3.20 illustrates the path of damage progression predicted by PDM as well as from experiments for the chosen panel configurations. For the first and second holes, failure propagates longitudinally from transverse edge of holes. Failure behavior near the third hole is found to be different from that of first and second hole. For the third hole, damage gets accumulated around the longitudinal edge of the hole. It can be clearly seen that PDM predictions match reasonably well with the experimental observations thereby confirming the accuracy of the implemented PDM. Further, it can be observed that the final failure modes of the first and second pin holes are shear-out mode. Bearing failure is observed near the third hole.

3.7.2 Effect of hole spacing on maximum stress value

Effect of hole spacing ratio, namely the ratio of longitudinal distance between the holes to pin diameter (F/D) and the ratio of transverse distance between the parallel holes to pin diameter (G/D) on the maximum stress value is investigated. Figure 3.21 illustrates the effect of hole spacing on maximum stress value for double-lap three-pin joint composite laminate. For G/D up to three, stress level reduces as F/D increases. It is because, the shielding effect provided by the third hole increases as F/D increases. The stress flux lines are diverted away from the first and second holes when the third hole is at a farther distance. For G/D more than three, stress level increases with increase in F/D as the shielding effect

69

of third hole diminishes. For *G/D* less than three, higher *F/D* is recommended and for *G/D* more than three, lower *F/D* is recommended. It can also be observed that, as *G/D* increases from 1.6 to 5.2 maximum stress value decreases. This is because of the lesser shielding effect provided by the third hole as the first and second holes moves farther. For *G/D* value more than 5.2, stress level increases because of the hole edge to specimen edge interaction. A *G/D* value of 5.2 is recommended since it gives lower stress values.

■ Matrix failure
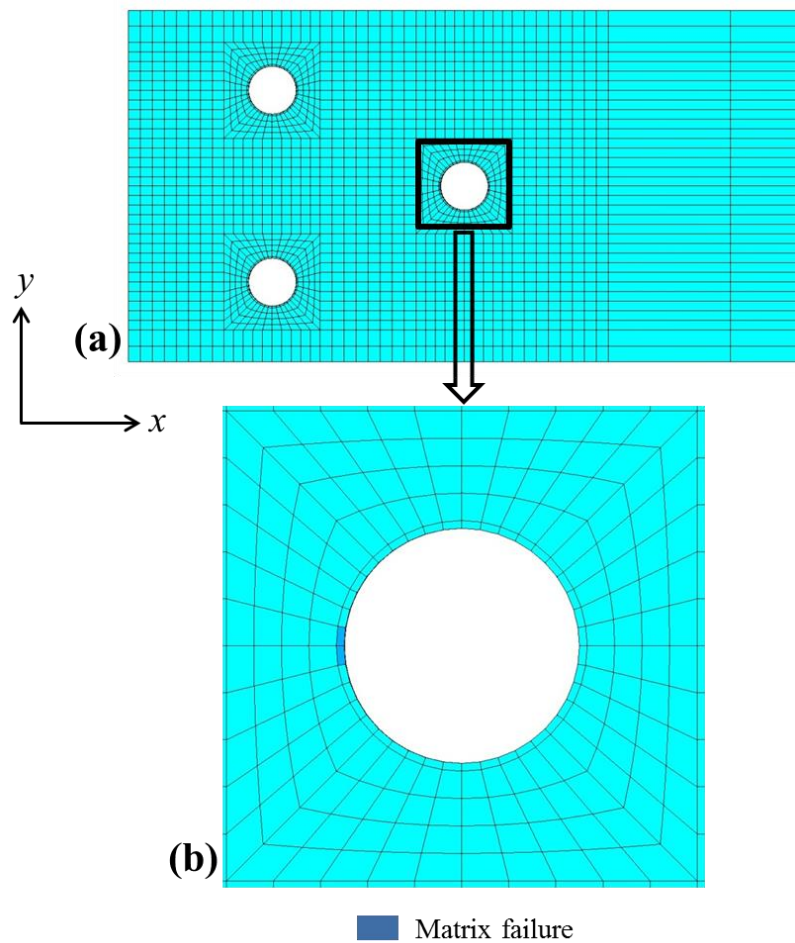
Figure 3.19: Failure initiation location in the middle panel predicted by PDM (a) overall view (b) zoomed up view showing failure initiation

Bearing failure   Shear out failure

- Fiber failure in tension
- Fiber failure in compression
- Matrix failure in tension
- Fiber-matrix shear failure
- More than on mode of failure

Figure 3.20: Damage propagation in the middle composite panel (a) Experiment (b) PDM prediction

Figure 3.21: Effect of hole spacing ratio on maximum stress (σ_{xx}) value

3.8   Closure

A 3D finite element based PDM is presented for double-lap, multi-pin joints in composite laminates subjected to in plane tensile load. A double-lap, three-pin joint in CFRP laminate is considered in this study. Hashin's failure criteria is used for damage prediction and material property degradation method is implemented for modeling the damage. Validation of the finite element model is performed by comparing whole field surface strains and displacements obtained from FEA with those from DIC technique. Good agreement is obtained between the FEA and DIC values. The PDM algorithm developed is able to predict different modes of failure, load – deflection behavior, damage progression up to final failure of the composite pin joint. It can also predict the final failure mode in the composite joint. Load – deflection behavior predicted by PDM is also compared with the experimental behavior and is found to be in good agreement. A deviation of 1.9 % is obtained in the final failure load predicted by PDM (for μ = 0.25) from the final failure load as observed in experiment. The location of failure initiation is found to be at the longitudinal edge of the third hole and the mode of failure initiation is matrix failure in tension. Path of damage progression predicted by PDM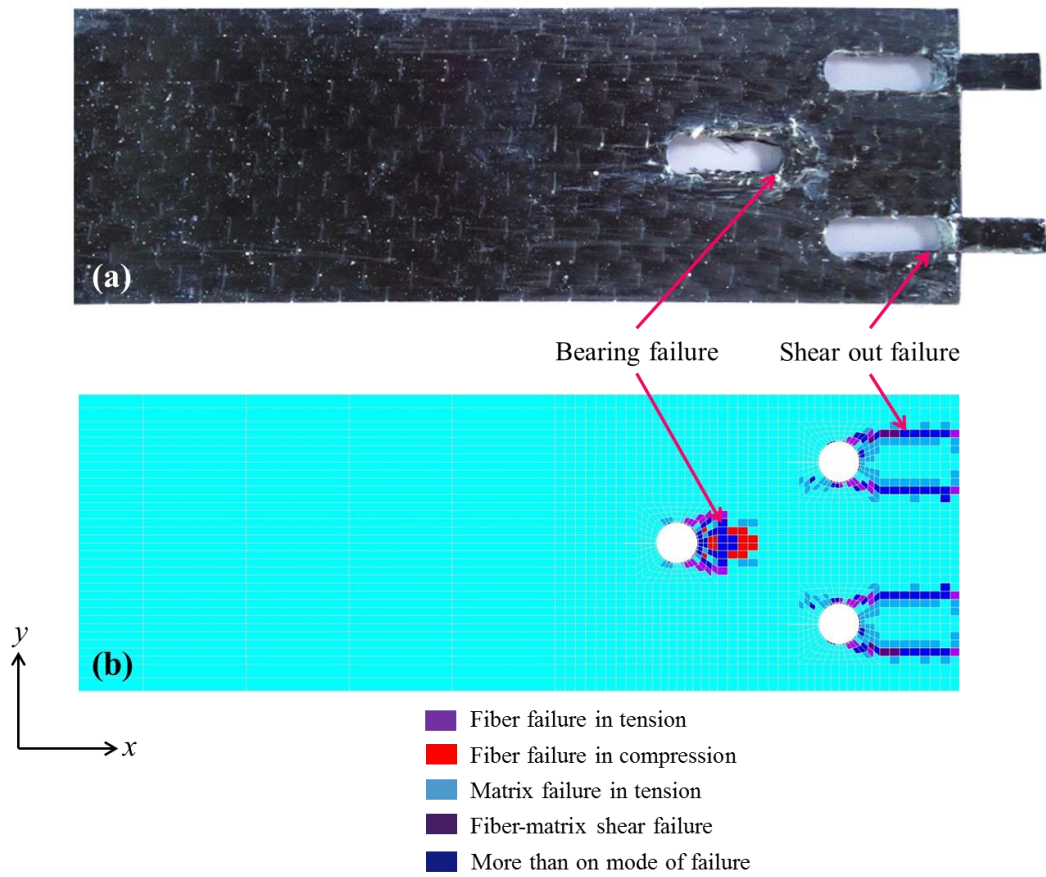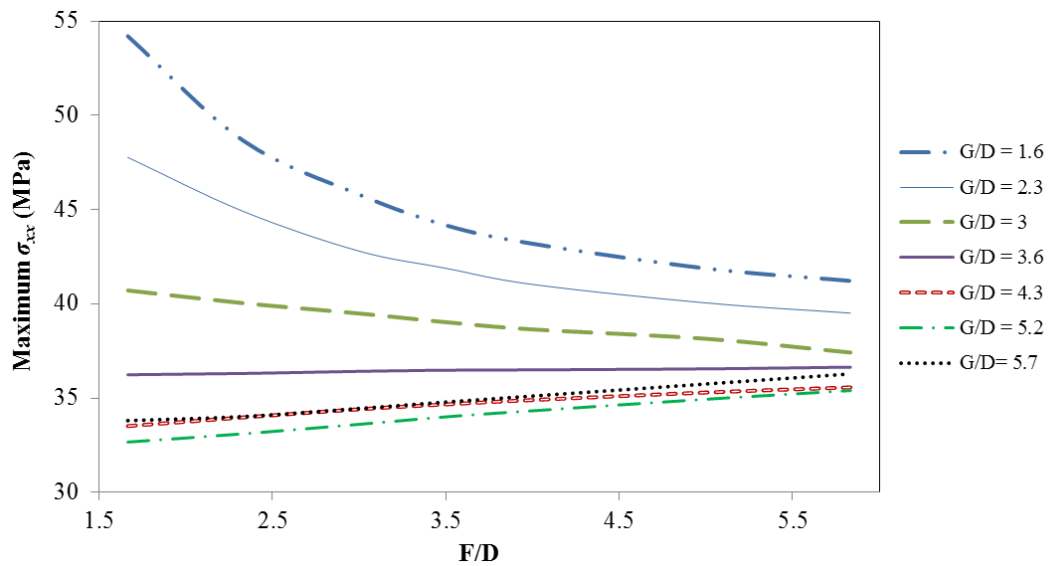 is also in coherence with the experimental observations thereby confirming the accuracy of the PDM algorithm developed. The final failure mode of the first and second pin holes is shear-out and final failure mode of the third hole is a bearing failure. Also, the effect of hole spacing ratio on the stress level in the panels is investigated further. For G/D less than 3, higher F/D is recommended and for G/D more than 3, lower F/D is recommended. A G/D value of 5.2 is recommended as it gives the least stress values.

Chapter 4

Conclusion and Recommendations for Future Work

In this work, a 3D finite element based progressive damage model is developed for fiber reinforced composite laminates and it is applied to CFRP laminates having multiple holes and also to multi-pin joints in CFRP laminates. The developed model is suitable for predicting failure and post failure behavior of the laminates. The three basic steps involved in PDM are stress analysis, failure analysis and damage propagation. Whole field surface strain analysis of the composite laminates is performed using digital image correlation experiments. Finite element model is first validated by comparing whole field surface strains and displacements obtained from FEA with those from DIC experiment. Load − deflection behavior predicted by PDM is also compared with the experimental behavior and is found to be in good agreement. Path of damage progression predicted by PDM is in line with the experimental observations there by confirming the accuracy of the PDM algorithm developed. For the multi-pin joints in CFRP laminates, the final failure modes predicted by PDM are in coherence with experimental observations. Effect of spacing between the holes on the maximum stress value in the panels is also further investigated and recommendations are made.

The variation of the load and displacement values predicted by PDM from experimentally observed values can be minimized by implementing a gradual stiffness reduction scheme rather than sudden stiffness reduction scheme used in this study. This gradual stiffness reduction scheme results in the partial unloading of elements and it allows repeated failures for the same element i.e. accumulation of damage in the element.

The study can be extended for progressive damage behavior of bolted joints in composite laminates. The contact between the panels, the washer and the panels and between the bolt and the surface of the hole need to be simulated. Pre-tension due to tightening effect needs to be applied on the bolt. It can be applied by giving first thermal expansion properties in the axial direction of the fastener and then decrease the temperature to create thermal stresses.

Further the present study is done for laminate under tensile load but it can be further extended for the compressive load case. Additional failure modes like buckling come into effect and it needs to be accurately predicted by PDM. Also it needs to be compared with experimental behavior.

Appendix A

Shear stress, shear strength and shear strain calculation

The in-plane shear strength for the ($\pm 45^0$) laminate is calculated using equation Eq. A.1. For estimating shear modulus, shear stress at each data point is also estimated using equation Eq. A.2 and shear strain using Eq. A.3.

$$\tau_{12}{}^m = \left(\frac{P^m}{2A} \right) \tag{A.1}$$

$$\tau_{12i} = \left(\frac{P_i}{2A} \right) \tag{A.2}$$

$$\gamma_{12i} = \varepsilon_{xi} - \varepsilon_{yi} \tag{A.3}$$

where, P^m and $\tau_{12}{}^m$ are the maximum load and maximum shear stress (shear strength) at or below 5% strain. P_i, τ_{12i} and γ_{12i} are the load, shear stress and shear strain at i^{th} data point. ε_{xi} and ε_{yi} are the longitudinal and lateral normal strains at i^{th} data point.

Appendix B
Out of plane properties evaluation

The orthotropic material is characterized by nine elastic constants namely E_{11}, E_{22}, E_{33}, G_{12}, G_{13}, G_{23}, v_{12}, v_{13} and v_{23}. Material axis system is illustrated in Figure B.1. The unidirectional fiber composite laminate is an orthotropic material in which fibers are in the 1–2 plane and the elastic properties are equal in 2–3 direction i.e., $E_{22} = E_{33}$, $G_{12} = G_{13}$, and $v_{12} = v_{13}$. However, the shear modulus G_{23} can be expressed in terms of E_{22} and v_{23} by Eq. B.1. Hence five independent elastic constants are needed to characterize the unidirectional fiber composites and can be considered as transverse isotropic [64]. The Poisson's ratio v_{21} is expressed in terms of v_{12} by Eq. B.2. Christensen [67] has shown that v_{23} can be related to v_{12} and v_{21} by Eq. B.3 in case of unidirectional fiber reinforced composites. Thus, unidirectional fiber reinforced composites can be characterized by four independent elastic constants.
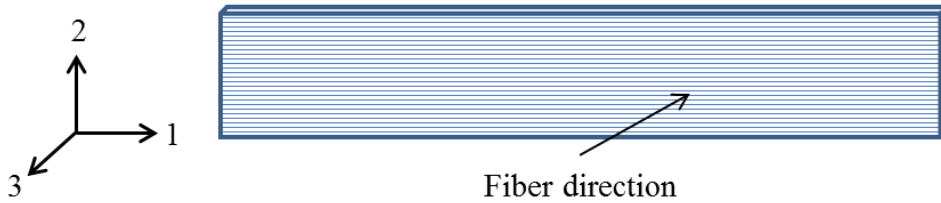

Figure B.1: Illustration of material axis system

$$G_{23} = \left(\frac{E_{22}}{2\left(1 + v_{23}\right)} \right) \tag{B.1}$$

$$v_{21} = v_{12} \left(\frac{E_{22}}{E_{11}} \right) \tag{B.2}$$

$$v_{23} = v_{12} \left(\frac{1 - v_{21}}{1 - v_{12}} \right) \tag{B.3}$$

where E, G and v are the Young's modulus, shear modulus and Poisson's ratio respectively.

References

[1] http://science-in-news.blogspot.in/2012/09/carbon-fibrea-new-era-in-aircraft-design.html

[2] http://www.skyscrapercity.com/showthread.php?t=933328&page=5

[3] Sr. Hallett and MR. Wisnom, Experimental Investigation of Progressive Damage and the Effect of Layup in Notched Tensile Tests, Journal of Composite Materials, 40(2), (2006) 119-141.

[4] J. Ubaid, M. Kashfuddoja and M. Ramji, Strength Prediction of cfrp Laminates with Multiple Interacting Holes, International Congress on Computational Mechanics and Simulation, Hyderabad, India (2012).

[5] B. Okutan, Stress and Failure Analysis of Laminated Composite Pin Joints, Doctoral Thesis, Graduate School of Natural and Applied Sciences, Dokuz Eziluz University, Singapore (2001).

[6] http://www.airliners.net/aviation-forums/general_aviation/read.main/3604483/

[7] PF. Liu and JY. Zheng, Recent Developments on Damage Modeling and Finite Element Analysis for Composite Laminates: A Review, Materials and Design, 31, (2010) 3825-3834.

[8] http://www.tech.plym.ac.uk/sme/mats324/

[9] A.C. Orifici, I. Herzberg and R.S. Thomson, Review of Methodologies for Composite Material Modeling Incorporating Failure, Composite Structures, 86, (2008) 194-210.

[10] C.G. Davila and P.P. Camanho, Failure Criteria for FRP Laminates in Plane Stress, NASA/TM, (2003) 212663.

[11] RG. Cuntze and A. Freund, The predictive capability of failure mode concept-based strength criteria for multidirectional laminates, Composite Science and Technology, 64, (2004) 344–377.

[12] R.M. Christensen, Tensor transformations and failure criteria for the analysis of fiber composite materials, Journal of Composite Materials, 22, (1988) 874–897.

[13] M.J. Hinton, A.S. Kaddour and P.D. Soden, Failure criteria in fibre reinforced polymer composites, Elsevier, Amsterdam, Netherlands (2004).

[14] Z. Hashin, Failure Criteria for Unidirectional Composites, Journal of Applied Mechanics, 47, (1980) 329–334.

[15] FK. Chang and KY Chang, A progressive damage model for laminated composites containing stress concentrations, Journal of Composite Materials, 21, (1987) 834-855.

[16] A. Puck, H. Schürmann, Failure analysis of FRP laminates by means of physically based phenomenological models, Composite Science and Technology, 58, (1998) 1045–67.

[17] R.M. Christensen, Stress based yield/failure criteria for fiber composites, International Journal of Solids and Structures, 34(5), (1997) 529–43.

[18] S.T. Pinho, C.G. Dávila, P.P. Camanho, L. Iannucci and P. Robinson, Failure models and criteria for FRP under in-plane or three-dimensional stress states including shear non-linearity. NASA/TM, (2005) 213530.

[19] Z. Hashin, A. Rotem, A fatigue failure criterion for fiber reinforced materials, Journal of Composite Materials 7, (1973) 448–64.

[20] R.S. Long, Static strength of adhesively bonded ARALL-1 joints, Journal of Composite Materials, 25, (1991) 391–415.

[21] L. Tong, An assessment of failure criteria to predict the strength of adhesively bonded composite double lap joints, Journal of Reinforced Plastic Composites, 16(8), (1997) 698–713.

[22] M.R. Wisnom, G.F.J. Hill and M.I. Jones, Through thickness failure prediction of composite structural elements. The 13th international conference on composite materials, Beijing, China. Paper no. 1623, 2001

[23] M. Grediac, The Use of Full-Field Measurement Methods in Composite Material Characterization: Interest and Limitations, Composites Part A, 35, (2004) 751-761.

[24] L.Toubal, M. Karama and B. Lorrain, Stress Concentration in A Circular Hole in Composite Plate, Composite Structures, 68, (2005) 31–36.

[25] MY. Tsai and J. Morton, An Investigation into the Stresses in Double-lap Adhesive Joints with Laminated Composite Adherends, Solids and Structures, 47, (2010) 3317–3325.

[26] RL. Hastie, R. Fredell, JW. Dally, A Photoelastic Study of Crack Repair, Experimental Mechanics, 38(1), (1998) 29-36.

[27] JD. Mathias, X. Balandraud, and M. Grediac, Experimental investigation of Composite Patches with A Full-field Measurement Method, Composites Part A: Applied Science and Manufacturing, 37, (2006) 177–190.

[28] MA. Sutton, J. Orteu and HW. Schreier, Image Correlation for Shape, Motion and Deformation Measurements: Basic Concepts, Theory and Applications, (Springer-Verlag, Berlin, 2009).

[29] B.Pan, K. Qian, H. Xie and A. Asundi, Two-dimensional Digital Image Correlation for In-plane Displacement and Strain Measurement: A Review, Measurement Science and Technology, 20, (2009) 062001 (17pp).

[30] S. Yoneyama and G. Murasawa, Digital Image Correlation, Experimental Mechanics (Freire, JF, ed.), (Eolss Publishers,2009).

[31] MA. Sutton, JH. Yan, V. Tiwari, HW. Schreier and JJ. Orteu, The effect of out-of-plane Motion on 2D and 3D Digital Image Correlation Measurements, Optics and Lasers in Engineering, 46, (2008) 746-757.

[32] Z.F. Zhang, Y.L. Kang, H.W. Wang, Q.H. Qin, Y. Qiu, and X.Q. Li, A novel coarse-fine search scheme for digital image correlation method. Measurement, 39(8), (2006) 710-718.

[33] Shi, X. Pang, H.L.J. Zhang, X.R. Liu, Q.J. and M. Ying, Components and Packaging Technologies, IEEE Transactions on, 27(4), (2004) 659-667.

[34] C.B. Wang, J. Deng, G.A. Ateshian, and C.T. Hung, An automated Method for Direct Measurement of Two-dimensional Strain Distributions within articular Cartilage under unconfined Compression, Journal of Biomechanical Engineering, 124, (2002) 557-567.

[35] G.F. Xiang, Q.C. Zhang, H.W. Liu, X.P. Wu, and X.Y. Ju, Time Resolved Deformation Measurements of the Portevin-Le Chatelier Bands, Scripta Materialia, 56, (2007) 721-724.

[36] B. Pan, A. Asundi, H. Xie and J. Gao, Digital image correlation using iterative least squares and pointwise least squares for displacement field and strain field measurements, Optics and Lasers in Engineering, 47, (2009) 865-874.

[37] S. Kazemahvazi, J. Kiele and D. Zenkert, Tensile strength of UD-composite laminates with multiple holes, Composites Science and Technology, 70(8), (2010) 1280–1287.

[38] E. Dan-Jumbo, R. Keller, WS. Chan and S. Selvaraj, Strength of composite laminate with multiple holes, 17th international conference on composite materials, Edinburgh, UK (2009).

[39] R. Manoharan and AK. Jeevanantham, stress and load-displacement analysis of fiber-reinforced composite laminates with a circular Hole under compressive load, Engineering and Applied Sciences 6 (4), (2011) 64-74.

[40] PP. Camanho and FL. Mathews, A progressive damage model for mechanically fastened joints in composite laminates, Journal of Composite Materials, 33, (1999) 2248-2280.

[41] D. Kermanidis, G. Labeas, KI. Tserpes and S. Pantelakis, Finite element modeling of damage accumulation in bolted composite joints under incremental tensile loading. European congress on computational methods in applied sciences and engineering, Barcelona, Spain (2000).

[42] CT. McCarthy, MA. McCarthy and VP. Lawlor, Progressive damage analysis of multi-bolt composite joints with variable bolt–hole clearances, Composites: Part B, 36, (2005) 290-305.

[43] F. Yang and CL. Chow, Progressive damage of unidirectional graphite/epoxy composites containing a circular hole, Journal of Composite Materials, 32, (1998) 504-525.

[44] P. Pal and C. Ray, Progressive failure analysis of laminated composite plates by finite element method, Reinforced Plastics and Composites, 21, (2002) 1505-1513.

[45] I. Lapczyk and JA. Hurtado, Progressive damage modeling in fiber-reinforced materials, Composites: Part A, 38, (2007) 2333-2341.

[46] RM. O'Higgins, MA. McCarthy and CT. McCarthy, Comparison of open-hole tension characteristics of high strength glass and carbon fibre-reinforced composite materials, Composites Science and Technology, 68, (2008) 2770-2778.

[47] TE. Tay, G. Liu, VBC. Tan, XS. Sun and DC. Pham, Progressive failure analysis of composites, Journal of Composite Materials, 42, (2008) 1921-1966.

[48] BM. Zhang and L. Zhao, Progressive damage and failure modeling in fiber-reinforced laminated composites containing a hole, International Journal of Damage Mechanics, 21, (2012) 893-911.

[49] NK. Hassan, MA. Mohamedien and SH. Riskallah, Finite element analysis of bolted connections for PFRP composites, Composites: Part B, 27B, (1996) 339-349.

[50] A. Aktas and R. Karakuzu, Failure Analysis of Two-Dimensional Carbon-Epoxy Composite Plate Pinned Joint, Mechanics of Composite Materials and Structures, 6(4), (1999) 347-361.

[51] T. Ireman, Design of Composite Structures Containing Bolt Holes and Open Holes, Doctoral Thesis, Department of Aeronautics, Royal Institute of Technology, Sweden (1999).

[52] KI. Tserpes, G. Labeas, P. Papanikos and Th. Kermanidis, Strength Prediction of Bolted Joints in Graphite/epoxy Composite Laminates, Composites Part B, 33, (2002) 521-529.

[53] I. Ilić, Numerical Simulation of Composite Structure Failure in the Areas of Geometric Discontinuities, Scientific Technical Review, Military Technical Institute, Serbia, LVIII(2), (2008) 32-36.

[54] AN. Kishore, SK. Malhotra and NS. Prasad, Failure analysis of multi-pin joints in glass fibre/epoxy composite laminates, Composite Structures, 91, (2009) 266-277.

[55] AA. Pisano, P. Fuschi, Mechanically Fastened Joints in Composite Laminates: Evaluation of Load Bearing Capacity, Composites: Part B, 42, (2011) 949-961.

[56] A. Aktas, Failure Analysis of Serial Pinned Joints in Composite Materials, Indian Journal of Engineering and Materials Science, 18, (2011) 102-110.

[57] AA. Pisano, P. Fuschi, D. De Domenico, Failure Modes Prediction of Multi-pin Joints FRP Laminates by Limit Analysis, Composites: Part B, 46, (2013) 197-206.

[58] WA. Samad, and RE. Rowlands, Non-destructive full field stress analysis of a composite structure containing an elliptical hole using digital image correlation. The joint international conference of the 2nd international symposium on experimental mechanics, the 11th asian conference on experimental mechanics, 2012 society for experimental mechanics fall conference and 7th international symposium on advanced science and technology in experimental mechanics, Taipei, Taiwan (2012).

[59] M. Kashfuddoja and M. Ramji, Experimental investigation of repaired CFRP laminates using 3D-DIC. The joint international conference of the 2nd international symposium on experimental mechanics, the 11th asian conference on experimental mechanics, 2012 society for experimental mechanics fall conference and 7th international symposium on advanced science and technology in experimental mechanics, Taipei, Taiwan (2012).

[60] M. Kashfuddoja, and M. Ramji, Whole-field Strain Analysis and Damage Assessment of adhesively bonded patch repair of CFRP Laminates using 3D-DIC and FEA, Composites Part B, 53, (2013) 46-61.

[61] Standard test method for tensile properties of polymer matrix composite materials. ASTM D3039/D 3039M-00.

[62] Standard test method for compressive properties of unidirectional or cross-ply fiber-resin composites. ASTM D3410.

[63] Standard test methods for in-plane shear response of polymer matrix composite materials by test of a ±45° laminate. ASTM D3518.

[64] P. Mallick, Fiber Reinforced Composites: Materials, Manufacturing, and Design, (CRC Press, New York, 2007).

[65] CM. Sanchez and MJ. Greene, Evaluation of Progressive Failure Analysis and Modeling of Impact Damage in Composite Pressure Vessels. Internship Report, NASA USRP (2011).

[66] DTG. Katerelos, M. Kashtalyan, C. Soutis and C. Galiotis, Matrix Cracking in Polymeric Composite Laminates: Modelling and Experiments, Composite Science and Technology, 68(12): (2008) 2310–2317.

[67] C. Zhang, R. Ganesan and SV. Hoa, Effects of friction on three-dimensional contact stresses in pin-loaded laminated composites. Journal of composite materials, 34(16), (2000)1382-1415.